

Precision Electroweak Constraints on Neutrinophilic Scalars

Saeid Foroughi-Abari ^a, Camilla Mupo ^a, Drona Vatsyayan ^{a,b} and Yue Zhang ^a

^a*Department of Physics, Carleton University, Ottawa, ON K1S 5B6, Canada*

^b*Arthur B. McDonald Canadian Astroparticle Physics Research Institute, 64 Bader Lane, Queen's University, Kingston, ON K7L 3N6, Canada*

E-mail: saeidf@physics.carleton.ca, camillamupo@mail.carleton.ca,
drona@physics.carleton.ca, y Zhang@physics.carleton.ca

ABSTRACT: Strong self-interaction among the active neutrinos mediated by a neutrinophilic scalar is a well-motivated target of particle physics and cosmological probes. In this article, we present precision electroweak constraints on models for neutrino self-interaction. We first work in the simplified model where the finite radiative corrections are obtained with the guidance of gauge invariance. These corrections are logarithmically enhanced for small mediator masses. We point out the importance of neutrino charged-current coupling correction and its impact on the Δr parameter and Fermi constant measurements. This effect was overlooked previously and allows us to derive the leading constraint on the neutrinophilic couplings for mediator mass above a few hundred MeV. We investigate the robustness of the result in a concrete UV completion which further includes a TeV-scale $SU(2)_L$ triplet scalar and find the simplified model constraints continue to hold for a wide range of parameter space. We pin down moving parts in the UV complete model and conditions when the contributions from heavy particle loops are no longer negligible. Our results serve as a useful road map for future explorations of the self-interacting neutrino paradigm.

Contents

1	Introduction	1
2	Impact of Neutrino Self-interaction on Electroweak Observables	4
2.1	The Fermi Constant	5
2.2	The Weak Mixing Angle	7
2.3	Z-Pole Observables	7
2.4	Non-Z-pole Observables	10
3	Precision Electroweak Constraint on Simplified Model	11
3.1	Global Fit for the SM	11
3.2	Global Fit for the Self-interacting Neutrino Scenario	13
3.2.1	Flavor-Universal Case	13
3.2.2	Flavor-Specific Cases	15
4	Complementary Constraints	16
5	Precision Electroweak Constraint on a UV Completion	17
5.1	Tree-level $Z \rightarrow \phi\phi^*$ Decay	19
5.2	Structure of Radiative Corrections to $\delta g_Z, \delta g_W$	19
5.3	Heavy T contribution to $\delta g_Z, \delta g_W$ and $Z\ell^+\ell^-$ Couplings	20
5.4	Constraints from Global Fit	24
5.5	Contribution to Electroweak Oblique Parameters	26
6	Conclusions and Outlook	29

1 Introduction

The neutrino sector bears a strong potential toward the next discovery of physics beyond the Standard Model (SM). Novel self-interaction among neutrinos is a well-motivated candidate of new physics for alleviating tensions in the cosmological data [1–8] and providing a viable production mechanism for sterile neutrino dark matter [9–14]. The strength of neutrino self-interaction is often parametrized using a dimensionful coupling G_{eff} (analogue of the Fermi constant) for low-energy scattering processes. Owing to the elusive nature of neutrinos, G_{eff} is allowed to be much higher than the actual Fermi constant. In terms of microscopic

theories, a large G_{eff} is enabled by the exchange of a light mediator (which will be called ϕ hereafter) with mass well below the weak scale. To avoid stringent constraints on the coupling to charged leptons (see *e.g.* [15, 16]), we consider ϕ to be neutrinophilic. The case of ϕ being a vector boson has been considered in [10, 17] and strong constraints are found for small ϕ masses due to enhanced longitudinal mode production. There is much more room for strong neutrino self-interaction if ϕ is a scalar boson [18]. At low energies, the interacting Lagrangian between ϕ and neutrino is given by

$$\mathcal{L} = \sum_{\alpha,\beta=e,\mu,\tau} \frac{\lambda_{\alpha\beta}}{2} \bar{\nu}_\alpha \mathbb{P}_R \nu_\beta^c \phi + \text{h.c.} \quad (1.1)$$

where $\nu_{\alpha,\beta}$ denote neutrinos contained in the SM lepton doublet and the superscript c means charge-conjugation. In this work, we assume that ϕ plays the sole role of mediating neutrino self-interaction and, for simplicity, it does not develop a vacuum expectation value (VEV).¹ This can be made technically natural if ϕ is a complex scalar and assigned two units of lepton number (or $B-L$) [19]. For the model to be phenomenologically viable,² the light ϕ must be (approximately) a singlet under the SM gauge symmetry. The Lagrangian Eq. (1.1) can be obtained from a gauge-invariant operator of the form $(\bar{L}_\alpha i\sigma_2 H^*)(H^\dagger i\sigma_2 L_\beta^c)\phi$, where L, H are the SM lepton and Higgs doublets. The Higgs VEV breaks $SU(2)_L$ and projects the neutrino field out of L , leading to the neutrinophilic interaction.

In this work, we explore one-loop radiative corrections arising from the above self-interaction and the corresponding predictions relevant for precision electroweak measurements. With low-energy experimental input on the fine-structure and Fermi constants, the per-mille level measurement of Z pole observables made by e^+e^- colliders (such as LEP-II and SLC) has served as a powerful tool for testing the electroweak gauge symmetry [20] and constraining various new physics candidates [21–25]. We apply it to derive an important constraint on the neutrino self-interaction parameter space.

To compute the radiative corrections to electroweak gauge couplings, one must go beyond the simplified model Eq. (1.1) by embedding it into a renormalizable and SM gauge invariant ultraviolet (UV) complete model. The cancellation of UV divergences is guaranteed by the Ward identity. The finite contribution can be divided into two parts, from loop diagrams involving ϕ , and those involving only heavy particles in the UV completion. While both parts have to vanish if the heavy particle mass scale M goes to infinity as dictated by the decoupling theorem, it was first suggested in [30] that the light ϕ contribution can

¹If ϕ had a VEV, it would contribute to the Majorana mass of neutrinos. In that case, the mass and coupling ranges of ϕ would be further restricted by the observed neutrino mixings and mass differences.

²*E.g.*, suppressing the contribution to Z -boson invisible width from the $Z \rightarrow \phi\phi^* \rightarrow \nu\nu\bar{\nu}$ decay channel, which will be discussed in detail in section 5.

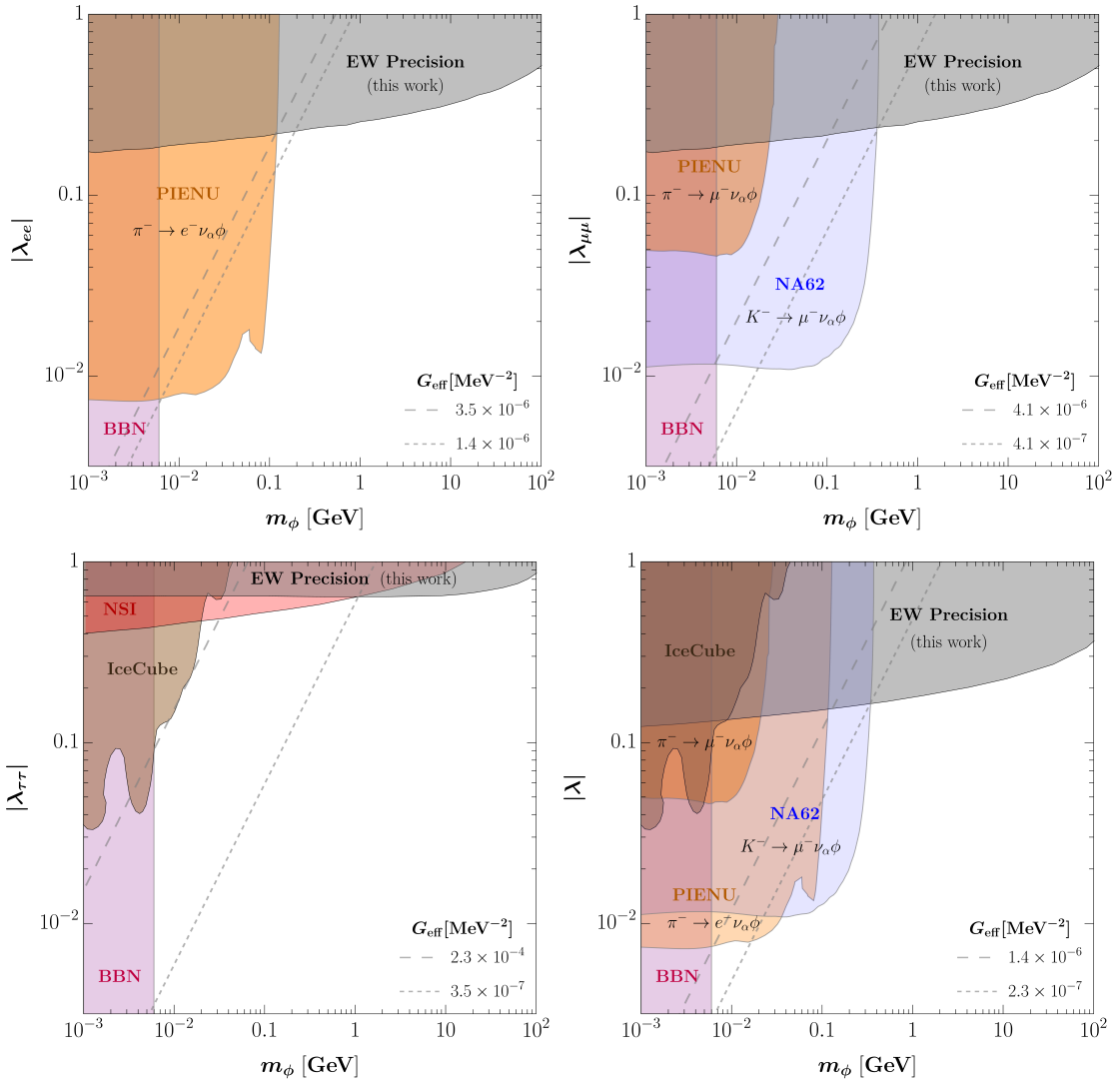


Figure 1. Constraints on neutrinophilic scalars mediating neutrino self-interaction for the flavor-specific and flavor-universal cases. The gray shaded regions excluded at the 2σ level from electroweak precision constraints are the main results of this work. The orange (blue) regions are ruled out from π^- (K^-) decay constraints set by PIENU [26] (NA62 [27]). The magenta shaded region represents the BBN bound: $m_\phi \geq 6$ MeV. In the ν_τ -specific case, the brown and red shaded regions correspond to the results derived from IceCube measurements [28], and constraints from non-standard neutrino interactions [29], respectively (see section 4 for details). The gray dashed and dotted lines are the contours of constant $G_{\text{eff}} \equiv \lambda^2/m_\phi^2$.

be relatively more important due to a logarithmic enhancement factor, $\ln(M^2/m_\phi^2)$. The presence of such a log factor is independent of details of the UV completion. We discuss its impact on electroweak physics in section 2. In particular, in cases where ϕ couples to ν_e or ν_μ , the radiative correction modifies the Fermi constant extracted from muon decay

and in turn affects Z -pole observations through the Δr parameter. This allows us to set the leading constraint for m_ϕ above ~ 300 MeV. In section 3, we perform a global fit to electroweak observables by altering the public `Gfitter` code [31, 32] to constrain the λ versus m_ϕ parameter space which is nearly model-independent in the light ϕ limit. We review some existing limits from charged meson decay and neutrino experiments in section 4. Together with the precision electroweak constraints, they allow us to chart the state-of-art probes of the self-interacting neutrino (SI ν) scenario in Fig. 1. In section 5, we calculate the heavy particle loop contribution to electroweak observables in a concrete UV completion that includes $SU(2)_L$ triplet scalar and discuss conditions for it to be subdominant to the light ϕ . We also point out that the electroweak oblique parameters can be used to further restrict the mass splitting among the triplet components, which is strongly correlated with the mass of light ϕ . We discuss the implication of our findings and conclude in section 6.

2 Impact of Neutrino Self-interaction on Electroweak Observables

The ϕ mediated neutrino self-interaction can affect the neutral and charged current interactions of neutrinos through radiative corrections. The electroweak Lagrangian reads

$$\mathcal{L} = -(g_Z)_{\alpha\beta} \bar{\nu}_\alpha \gamma^\mu \mathbb{P}_L \nu_\beta Z_\mu - \left[(g_W)_{\alpha\beta} \bar{\ell}_\alpha \gamma^\mu \mathbb{P}_L \nu_\beta W_\mu^- + \text{h.c.} \right], \quad (2.1)$$

where $\mathbb{P}_{L,R} = (1 \mp \gamma_5)/2$. At tree level, the couplings are flavor diagonal ($\alpha = \beta$), $g_Z^0 = g/(2 \cos \theta_W)$, $g_W^0 = g/\sqrt{2}$, where θ_W denotes the weak mixing angle and g is the $SU(2)_L$ gauge coupling.

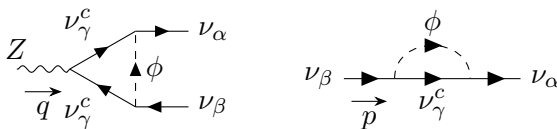


Figure 2. Feynman diagrams through which a light neutrinophilic ϕ affects the neutrino neutral and charged current interactions at one-loop level.

The presence of a neutrinophilic scalar ϕ contributes to the radiative corrections through the vertex and self-energy diagrams in Fig. 2. Because Eq. (1.1) is not gauge invariant under $SU(2)_L \times U(1)_Y$, the light ϕ contribution alone has UV divergences. This problem can be solved by resorting to a gauge invariant UV complete model that contains new heavy particles (with mass scale M above the electroweak scale). Inclusion of the new particle loop diagrams renders the result UV finite. Regardless of the form of UV completion, the

light ϕ contributions to neutrino electroweak couplings take the generic form [30]

$$\begin{aligned}(\delta g_Z)_{\alpha\beta} &= -\frac{g_Z^0 \lambda_{\alpha\gamma} \lambda_{\beta\gamma}^*}{32\pi^2} \left[\ln \frac{M^2}{m_\phi^2} + c_Z + f_1(q^2, m_\phi, M) + \mathcal{O}\left(\frac{1}{M^2}\right) \right], \\(\delta g_W)_{\alpha\beta} &= -\frac{g_W^0 \lambda_{\alpha\gamma} \lambda_{\beta\gamma}^*}{64\pi^2} \left[\ln \frac{M^2}{m_\phi^2} + c_W + \mathcal{O}\left(\frac{1}{M^2}\right) \right],\end{aligned}\tag{2.2}$$

where q^μ is the momentum carried by the Z boson. The $\mathcal{O}(1/M^2)$ terms are negligible for $|q^2|, m_\phi^2 \ll M^2$. The dummy flavor index γ is summed over.

Both δg_Z and δg_W contain a logarithmic factor which can be large if m_ϕ lies well below the electroweak scale. The constants c_Z, c_W are order one numbers whose exact values depend on the details of the UV completion. In the scalar triplet model to be discussed below, it has been found that $c_Z = -11/2$ and $c_W = -2$ [29]. For light ϕ they are subdominant to the log factor. The finite loop function f_1 reads

$$f_1(q^2, m_\phi, M) \equiv 2\text{Re} \int_0^1 dx \int_0^{1-x} dy \left[\ln \left(\frac{M^2}{(1-x-y)m_\phi^2 - xyq^2} \right) + \frac{xyq^2}{(1-x-y)m_\phi^2 - xyq^2} \right].\tag{2.3}$$

The q^2 dependence in the neutral-current coupling δg_Z and the interplay with m_ϕ^2 has been explored in [29, 30]. In this work, we point out the importance of the correction δg_W in the precision electroweak constraints. We will consider flavor diagonal λ couplings ($\alpha = \beta$) throughout this work. As a result, the gauge couplings $g_{W,Z}$ stay flavor diagonal.

Besides Eq. (2.2), there could be additional contributions to $\delta g_{Z,W}$ from heavy particle loops that do not involve ϕ . We will address their importance in section 5 in the context of a concrete UV complete model.

2.1 The Fermi Constant

The Fermi constant is defined as $G_F \equiv \sqrt{2}g^2/(8m_W^2)$ and is most precisely determined by measuring the muon lifetime τ_μ . For nonzero λ_{ee} and/or $\lambda_{\mu\mu}$, the correction to g_W affects the charged-current process. It is useful to define the new physics contribution to the Δr parameter

$$\Delta r^{\text{SI}\nu} \equiv \frac{(\delta g_W)_{ee} + (\delta g_W)_{\mu\mu}}{g_W^0} = -\frac{|\lambda_{ee}|^2 + |\lambda_{\mu\mu}|^2}{64\pi^2} \left(\ln \frac{M^2}{m_\phi^2} + c_W \right).\tag{2.4}$$

The corresponding muon lifetime reads

$$\frac{1}{\tau_\mu} \simeq \left(1 + \Delta r^{\text{SI}\nu} \right)^2 \left(\frac{1}{\tau_\mu} \right)_{\text{SM}}.\tag{2.5}$$

This expression is precise for $m_\phi > m_\mu$. For $m_\phi \ll m_\mu$, a four-body muon decay channel opens up where ϕ can be radiated from a final state neutrino. In the $m_\phi \rightarrow 0$ limit, it

needs to be added to the three-body decay rate to render the total width finite.³ Our precision electroweak analysis does not include the four-body decay contribution because for the mass range $m_\phi < m_\mu$, other constraints (from the exotic decays of charged meson to ϕ) are much stronger, as shown in Fig. 1.

For nonzero $\Delta r^{\text{SI}\nu}$, the extracted G_F value from muon lifetime depends on the strength of neutrino self-interaction

$$G_F = \frac{G_\mu}{1 + \Delta r^{\text{SI}\nu}} \simeq (1 - \Delta r^{\text{SI}\nu})G_\mu , \quad (2.6)$$

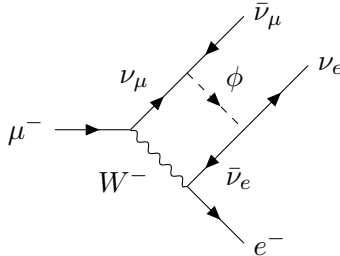
where the second step is valid because $|\Delta r^{\text{SI}\nu}| \ll 1$. Throughout this work, we define

$$G_\mu \equiv 1.16637 \times 10^{-5} \text{ GeV}^{-2} . \quad (2.7)$$

This value is fixed by the muon lifetime measurement, which contains both the SM Fermi constant and the new physics correction $\Delta r^{\text{SI}\nu}$.

In the SM limit, $\Delta r^{\text{SI}\nu} = 0$, thus $G_F = G_\mu$. It is useful to note from Eq. (2.4) that $\Delta r^{\text{SI}\nu}$ is negative for very light ϕ . Therefore, the presence of neutrino self-interaction increases the value of G_F extracted from muon lifetime measurement.

It is also useful to note that if both λ_{ee} and $\lambda_{\mu\mu}$ are nonzero, the ϕ exchange can induce an exotic muon decay through a box diagram as shown below. Because ϕ carries lepton number, the decay final state is $e^- \nu_e \bar{\nu}_\mu$. As a result, this box diagram does not interfere with the tree-level one. The corresponding correction to G_F occurs at $\mathcal{O}(\lambda^4)$ and is subdominant to $\Delta r^{\text{SI}\nu}$ which is $\mathcal{O}(\lambda^2)$. We do not take it into account in our analysis.



The G_F measurement using muon lifetime alone cannot constrain new physics. However, there are other ways to precisely determine G_F from the measurement of other electroweak observables. In the SM, the agreement is at the per mille level, which demonstrates the success of the $SU(2) \times U(1)$ gauge theory and tightly restricts the room for new physics [33]. Alternatively, one can use the G_F extracted from muon lifetime as an input to construct other electroweak observables. The information of neutrino self-interaction will be encoded in the prediction of those observables and impact the global fit to the experimental data.

³The $m_\phi \rightarrow 0$ limit and infrared safety is only an academic question given the ΔN_{eff} constraint from big-bang nucleosynthesis which requires m_ϕ to be above MeV scale.

2.2 The Weak Mixing Angle

In the SM, the weak mixing angle is related to the fine-structure constant, the Fermi constant, and the physical mass of Z boson as [33]

$$\sin^2 \theta_W^{\text{SM}} \cos^2 \theta_W^{\text{SM}} = \frac{\pi\alpha}{\sqrt{2}G_\mu m_Z^2 (1 - \Delta r^{\text{SM}})}, \quad (2.8)$$

where Δr^{SM} accounts for radiative corrections to this relationship [34]. For clarity, both $\sin^2 \theta_W$ and Δr are defined using the on-shell renormalization scheme, which is consistent with the convention used by the `Gfitter` package. In the presence of neutrino self-interaction, we have to replace G_μ by G_F given in Eq. (2.6) and the new weak mixing angle is related to its SM counterpart as

$$\sin^2 \theta_W \cos^2 \theta_W = \frac{\sin^2 \theta_W^{\text{SM}} \cos^2 \theta_W^{\text{SM}}}{1 - \Delta r^{\text{SI}\nu}} \simeq \frac{\pi\alpha}{\sqrt{2}G_\mu m_Z^2 (1 - \Delta r^{\text{SM}} - \Delta r^{\text{SI}\nu})}. \quad (2.9)$$

With $|\Delta r^{\text{SI}\nu}| \ll 1$, we can further derive

$$\sin \theta_W \simeq \sin \theta_W^{\text{SM}} \left[1 + \frac{1 + \sec(2\theta_W^{\text{SM}})}{4} \Delta r^{\text{SI}\nu} \right]. \quad (2.10)$$

Eqs. (2.6) and (2.10) represent the contribution of neutrino self-interaction to the electroweak sector through the Δr parameter. If this were the only effect, one could already apply the 2σ limit

$$|\Delta r^{\text{SI}\nu}| < 0.0012, \quad (2.11)$$

given in [35] to set an upper bound on λ as a function of m_ϕ . However, as we will see below, neutrino self-interaction also impacts electroweak observables in other ways, through the radiative correction to δg_Z , as well as directly contributing to new decay channels with light ϕ in the final state. A more careful analysis is required and presented below.

2.3 Z -Pole Observables

The Z -boson pole observables have been measured to very high precision, primarily by the LEP and SLC experiments [36, 37]. These include the mass (m_Z), the total decay width of Z -boson (Γ_Z), partial decay widths and their ratios (R_i), the asymmetry parameters (A_i), the total hadronic cross-section (σ_{had}^0), and the effective weak mixing angle ($\sin^2 \theta_{\text{eff}}^\ell$). Their measured values are listed in the second column of Table 1. Here we discuss how they are affected by neutrino self-interaction.

- The Z boson mass $m_Z = 91.188$ GeV is used as an input in our analysis.

- Due to parity violation in the EW sector, the initial and final state fermion polarizations in neutral current interactions such as $e^+e^- \rightarrow f\bar{f}$ have an observable asymmetry that is given by the asymmetry parameters

$$A_f = \frac{2g_{V,f}g_{A,f}}{g_{V,f}^2 + g_{A,f}^2}, \quad (2.12)$$

where f denotes SM fermions, $f = e, \mu, \tau, b, c, s$, and

$$g_{V,f} = \sqrt{\rho_Z^f} \left(I_3^f - 2Q^f \kappa_Z^f \sin^2 \theta_W \right), \quad g_{A,f} = \sqrt{\rho_Z^f} I_3^f, \quad (2.13)$$

are the vector and axial couplings of the Z -boson to fermions. The electroweak form factors ρ_Z^f, κ_Z^f , which are equal to unity at the tree level, encode the radiative corrections evaluated on the Z -pole [38]. In the simplified neutrino self-interaction model Eq. (1.1), the new corrections to ρ_Z^f and κ_Z^f occur beyond one-loop level due to the neutrinophilic nature of ϕ , unless $f = \nu$. The leptonic asymmetries are combined into a single observable A_l assuming lepton flavour universality, leaving us with 4 observables: A_l, A_b, A_c and A_s . These asymmetry parameters are affected by $\Delta r^{\text{SI}\nu}$ through the weak mixing angle Eq. (2.10).

- The above asymmetry parameters are used to construct the forward-backward asymmetry as

$$A_{\text{FB}}^f = \frac{\sigma_F^f - \sigma_B^f}{\sigma_F^f + \sigma_B^f} = \frac{3}{4} A_e A_f, \quad (2.14)$$

where $\sigma_{F,B}^f$ is the fermionic production cross-section in the forward/backward hemisphere relative to the electron beam direction. Similarly, A_{FB}^f is also affected by neutrino self-interaction through the weak mixing angle.

- The effective weak mixing angle ($\sin^2 \theta_{\text{eff}}^\ell$) on the Z -pole is related to the $\sin^2 \theta_W$ in Eq. (2.10) as [39]

$$\sin^2 \theta_{\text{eff}}^\ell = \kappa_Z^\ell \sin^2 \theta_W. \quad (2.15)$$

It has been measured using charge flow (Q_{FB}) at LEP [36] and recently at hadron colliders (HC) including the Tevatron and LHC [40–43].

- The Z boson total decay width is given by

$$\Gamma_Z = \Gamma_Z^{\text{SM}} (\Delta r^{\text{SI}\nu}) + \delta\Gamma_{Z \rightarrow \nu\bar{\nu}} + (\Gamma_{Z \rightarrow \nu\nu\phi^*} + \Gamma_{Z \rightarrow \bar{\nu}\bar{\nu}\phi}), \quad (2.16)$$

where the SM decay width is given by $\Gamma_Z^{\text{SM}} = \Gamma_e + \Gamma_\mu + \Gamma_\tau + 3\Gamma_\nu + \Gamma_{\text{had}}$ and $\Gamma_{\text{had}} = \Gamma_u + \Gamma_d + \Gamma_s + \Gamma_c + \Gamma_b$. The partial decay widths are written in terms of G_F and

$\sin\theta_W$ (see Eq. (21) in Ref. [31]). In the presence of neutrino self-interaction, both G_F and $\sin\theta_W$ are affected by $\Delta r^{\text{Sl}\nu}$ as given by Eqs. (2.6) and (2.10).

- The neutrino final state requires special care in the presence of self-interaction. In Eq. (2.16), the second term on the right-hand side, $\delta\Gamma_{Z\rightarrow\nu\bar{\nu}}$ accounts for the shift to $Z\rightarrow\nu\bar{\nu}$ decay width (summing over all flavors) due to the radiative correction to neutrino neutral current coupling, δg_Z given by Eq. (2.2). Essentially, δg_Z shifts the electroweak form factor ρ_Z^ν as

$$\left(\sqrt{\rho_Z^{\nu\alpha}} - 1\right)_{\text{Sl}\nu} = \frac{\text{Re}(\delta g_Z)_{\alpha\alpha}}{g_Z^0}. \quad (2.17)$$

This partial width shift has been calculated in [29] (see also [44]) and

$$\begin{aligned} \delta\Gamma_{Z\rightarrow\nu\bar{\nu}} &\simeq \Gamma_{Z\rightarrow\nu\alpha\bar{\nu}\alpha}^{\text{SM, tree}} \cdot \frac{2\text{Re}(\delta g_Z)_{\alpha\alpha}}{g_Z^0} \\ &= -\frac{\sqrt{2}G_\mu m_Z^3 |\lambda_{\alpha\alpha}|^2}{384\pi^3} \left[\ln \frac{M^2}{m_\phi^2} + \text{Re} f_1(q^2 = m_Z^2, m_\phi, M) + c_Z \right], \end{aligned} \quad (2.18)$$

where $\Gamma_{Z\rightarrow\nu\alpha\bar{\nu}\alpha}^{\text{SM, tree}} = G_\mu m_Z^3 / (12\sqrt{2}\pi)$ and the flavor index $\alpha = e, \mu, \tau$ is summed over. Here, we do not have to distinguish between G_F and G_μ because the contribution is already at $\mathcal{O}(\lambda^2)$ order. The last bracket of Eq. (2.16) is a new three-body decay channel of the Z boson with an on-shell ϕ (or ϕ^*) in the final state. Because ϕ eventually decays into neutrinos, the final state is also invisible. The three-body decay rate is [29]

$$\begin{aligned} \Gamma_{Z\rightarrow\nu\nu\phi^*} + \Gamma_{Z\rightarrow\bar{\nu}\bar{\nu}\phi} &= \frac{\sqrt{2}G_\mu m_Z^3 |\lambda_{\alpha\alpha}|^2}{192\pi^3} \left\{ \left(\ln \frac{m_Z^2}{m_\phi^2} - \frac{11}{3} \right) + \frac{8m_\phi^2}{m_Z^2} \left(\ln \frac{m_Z^2}{m_\phi^2} - \frac{5}{8} \right) \right. \\ &\left. + \frac{2m_\phi^4}{m_Z^4} \left[\ln \frac{m_Z^2}{m_\phi^2} \left(\ln \frac{m_Z m_\phi}{m_Z^2 + m_\phi^2} + \frac{3}{2} \right) + \frac{9}{2} + \text{Li}_2 \left(\frac{m_Z^2}{m_Z^2 + m_\phi^2} \right) - \text{Li}_2 \left(\frac{m_\phi^2}{m_Z^2 + m_\phi^2} \right) \right] - \frac{m_\phi^6}{3m_Z^6} \right\}. \end{aligned} \quad (2.19)$$

Again, the flavor index α is summed over. In the $m_\phi \ll m_Z$ limit,

$$\delta\Gamma_{Z\rightarrow\nu\bar{\nu}} + (\Gamma_{Z\rightarrow\nu\nu\phi^*} + \Gamma_{Z\rightarrow\bar{\nu}\bar{\nu}\phi}) \simeq -\frac{G_\mu m_Z^3 |\lambda_{\alpha\alpha}|^2}{96\sqrt{2}\pi^3} \left(\ln \frac{M^2}{m_Z^2} + \frac{17 + 3c_Z}{6} \right), \quad (2.20)$$

which is independent of m_ϕ . If $\Delta r^{\text{Sl}\nu} \neq 0$, the remaining $\ln(M^2/m_\phi^2)$ enhancement resides in the first term of Eq. (2.16) which makes the dominant correction to the total Z width.

- The remaining observables are the partial width ratios and total hadronic cross-section at Z pole, defined as

$$R_\ell = \frac{\Gamma_{\text{had}}}{\Gamma_\ell}, \quad R_q = \frac{\Gamma_q}{\Gamma_{\text{had}}}, \quad \sigma_{\text{had}} = \frac{12\pi}{m_Z^2} \frac{\Gamma_e \Gamma_{\text{had}}}{\Gamma_Z^2}, \quad (2.21)$$

where $q = b, c, s$. In the presence of neutrino self-interaction, all of these partial decay widths, and in turn R_ℓ , R_q and σ_{had} , receive correction from $\Delta r^{\text{SI}\nu}$ through G_F and $\sin \theta_W$.

2.4 Non- Z -pole Observables

The two main W -boson observables are its mass and decay width determined from the combination of the experiments at Tevatron and LHC [45–47]. Their values are given in the second column of Table 1.

The physical masses of W, Z bosons are used to define the weak mixing angle

$$m_W \equiv m_Z \cos \theta_W , \quad (2.22)$$

θ_W is given by Eq. (2.10) and depends on neutrino self-interaction through $\Delta r^{\text{SI}\nu}$, and with m_Z as input, so does the W mass. Under the on-shell renormalization scheme, the above relation holds to all orders of perturbation theory [20].

Similar to Z boson, the total decay width of the W boson can be written as

$$\Gamma_{W^-} = \Gamma_{W^-}^{\text{SM}} (\Delta r^{\text{SI}\nu}) + \delta\Gamma_{W^- \rightarrow \ell \bar{\nu}} + \Gamma_{W^- \rightarrow \ell \nu \phi^*} . \quad (2.23)$$

The SM W decay width is written in terms of G_F and m_W (see Eq. (20) of [48]). In the presence of neutrino self-interaction, both are affected by $\Delta r^{\text{SI}\nu}$ via Eqs. (2.6) and (2.22).

The radiative correction to g_W makes an additional contribution to the leptonic decay amplitude of the W boson, denoted as $\delta\Gamma_{W^- \rightarrow \ell \bar{\nu}}$ in Eq. (2.23). We find

$$\delta\Gamma_{W \rightarrow \ell \bar{\nu}} \simeq \Gamma_{W \rightarrow \ell \bar{\nu}}^{\text{SM, tree}} \cdot \frac{2(\delta g_W)_{\alpha\alpha}}{g_W^0} = -\frac{G_\mu m_W^3 |\lambda_{\alpha\alpha}|^2}{192 \sqrt{2} \pi^3} \left(\ln \frac{M^2}{m_\phi^2} + c_W \right) , \quad (2.24)$$

where $\Gamma_{W \rightarrow \ell \bar{\nu}}^{\text{SM, tree}} = G_\mu m_W^3 / (6\sqrt{2}\pi)$. A light ϕ can also be radiated from final state neutrino, leading to a three-body decay mode of the W boson

$$\Gamma_{W \rightarrow \ell \nu \phi^*} = \frac{G_\mu m_W^3 |\lambda_{\alpha\alpha}|^2}{1152 \sqrt{2} \pi^3} \left[-17 + 9 \left(\frac{m_\phi^2}{m_W^2} + \frac{m_\phi^4}{m_W^4} \right) + 6 \left(1 + 3 \frac{m_\phi^2}{m_W^2} \right) \ln \frac{m_W^2}{m_\phi^2} - \frac{m_\phi^6}{m_W^6} \right] , \quad (2.25)$$

which is kinematically allowed for $m_\phi < m_W$, and we have neglected the charged lepton masses. In both Eqs. (2.24) and (2.25), the flavor index α is summed over e, μ, τ . In the $m_\phi \ll m_W$ limit,

$$\delta\Gamma_{W \rightarrow \ell \bar{\nu}} + \Gamma_{W \rightarrow \ell \nu \phi} \simeq -\frac{G_\mu m_W^3 |\lambda_{\alpha\alpha}|^2}{192 \sqrt{2} \pi^3} \left(\ln \frac{M^2}{m_W^2} + \frac{17 + 2c_W}{6} \right) . \quad (2.26)$$

The $\ln(M^2/m_\phi^2)$ enhancement factor is absent here, similar to the case of Z decay.

3 Precision Electroweak Constraint on Simplified Model

The global fit of the predictions to the electroweak precision data is not only instrumental for validating the gauge structure of the SM but also provides powerful tests of beyond the SM physics. Given the radiative corrections to both charged- and neutral-current interactions from a neutrinophilic scalar, it becomes even more pertinent to use a fitting program to determine the precision constraints, instead of just constraining the Z decay width as was done in previous works [29, 49].

We adopt and modify the `Gfitter` package [31, 32] to include the effects from the self-interacting neutrino sector, including the simplified model that contains a neutrinophilic scalar, as well as a UV completion to be discussed in section 5. The package follows a frequentist approach to find the global minimum of square (χ^2_{\min}), with the test statistic for a set of model parameters y_i defined by

$$\chi^2(y_i) \equiv -2 \ln \mathcal{L}(y_i), \quad (3.1)$$

where \mathcal{L} is the likelihood function.

3.1 Global Fit for the SM

We begin with a telegraphic review of the SM global fit. The following input parameters are allowed to float within their experimentally determined range

$$y_i = \{\alpha_s(m_Z^2), \Delta\alpha_{\text{had}}^{(5)}(m_Z^2), m_Z, m_t, M_H\}, \quad (3.2)$$

where $\alpha_s(m_Z^2)$ is the strong coupling constant, $\Delta\alpha_{\text{had}}^{(5)}$ is the hadronic contribution of the light five quarks to the electromagnetic coupling constant (evaluated at the m_Z scale), m_t is the top mass and M_H is the SM Higgs boson mass. Along with these parameters, the other floating parameters are the quark masses: $\{m_c, m_b\}$. The lighter quark masses have been precisely determined by lattice QCD [50, 51] and are kept fixed in the fit, along with $G_F = G_\mu$ measured using the muon lifetime.

The `Gfitter` code incorporates theoretical computations up to full two-loop and beyond-two-loop corrections for $m_W, \sin^2 \theta_{\text{eff}}^\ell$, partial and total Z decay widths [48, 52–54]. The missing higher order corrections are all encapsulated via theoretical uncertainty parameters [31, 55]

$$\begin{aligned} \delta_{\text{th}} m_W &= 4 \text{ MeV}, \quad \delta_{\text{th}} \sin^2 \theta_{\text{eff}}^f = 4.7 \times 10^{-5}, \quad \delta_{\text{th}} \Gamma_Z = 0.4 \text{ MeV}, \quad \delta_{\text{th}} \sigma_{\text{had}} = 6 \text{ pb}, \\ \delta_{\text{th}} R_\ell &= 0.6, \quad \delta_{\text{th}} R_b = 0.0001, \quad \delta_{\text{th}} R_c = 0.00005. \end{aligned} \quad (3.3)$$

All the electroweak observables contributing to the global fit, along with their input values, are given in first and second columns of Table 1. The experimental uncertainties

		SM		SI ν (Universal)	
Parameter	Input value	Fit	Pull	Fit	Pull
$\alpha_s(m_Z^2)$	0.1177 ± 0.0009	0.118 ± 0.0009	+0.37	0.1180 ± 0.0008	+0.33
$\Delta\alpha_{\text{had}}^{(5)}(m_Z^2)^{(\Delta)}$	0.02758 ± 0.00010	0.02757 ± 0.00009	-0.17	0.02756 ± 0.0001	-0.27
m_Z [GeV]	91.188 ± 0.0020	91.1885 ± 0.0020	+0.25	91.1885 ± 0.0020	+0.25
m_t [GeV]	172.56 ± 0.61	172.70 ± 0.58	+0.20	172.81 ± 0.8	+0.35
M_H [GeV]	125.1 ± 0.1	125.1 ± 0.1	0.00	125.1 ± 0.00	0.00
m_W [GeV]	80.369 ± 0.013	80.358 ± 0.006	-0.86	80.362 ± 0.007	-0.55
Γ_W [GeV]	2.140 ± 0.050	2.090 ± 0.001	-1.00	2.091 ± 0.001	-0.98
$\sin^2 \theta_{\text{eff}}^\ell(\text{HC})$	0.23152 ± 0.00023	0.23152 ± 0.00006	0.00	0.23152 ± 0.00006	+0.26
$\sin^2 \theta_{\text{eff}}^\ell(Q_{\text{FB}})$	0.2324 ± 0.0012	0.23152 ± 0.00006	-0.73	0.23152 ± 0.00006	-0.68
$A_\ell(\text{LEP})$	0.1465 ± 0.0033	0.1470 ± 0.0004	+0.15	0.1470 ± 0.0004	-0.02
$A_\ell(\text{SLD})$	0.1513 ± 0.0021	0.1470 ± 0.0004	-2.05	0.1468 ± 0.0004	-2.26
Γ_Z [GeV]	2.4955 ± 0.0023	2.4945 ± 0.0005	-0.43	2.4940 ± 0.0006	-0.65
σ_{had} [nb]	41.480 ± 0.033	41.489 ± 0.008	+0.27	41.489 ± 0.004	+0.27
R_ℓ	20.767 ± 0.025	20.733 ± 0.006	-1.35	20.733 ± 0.005	-1.38
A_{FB}^ℓ	0.0171 ± 0.0010	0.01620 ± 0.0001	-0.90	0.01610 ± 0.0002	-1.00
R_b	0.21629 ± 0.00066	0.21582 ± 0.00003	-0.70	0.21583 ± 0.00003	-0.71
R_c	0.1721 ± 0.0030	0.17220 ± 0.00003	+0.04	0.17222 ± 0.00002	+0.04
A_{FB}^b	0.0996 ± 0.0016	0.1030 ± 0.0003	+2.13	0.1027 ± 0.0005	+1.94
A_{FB}^c	0.0707 ± 0.0035	0.0736 ± 0.0002	+0.83	0.0733 ± 0.0004	+0.74
A_b	0.923 ± 0.020	0.93462 ± 0.00003	+0.58	0.93458 ± 0.00006	+0.58
A_c	0.670 ± 0.027	0.6678 ± 0.00019	-0.08	0.6677 ± 0.0003	-0.09
$ \lambda $	[0.001 - 1.0]	-	-	0.064 ± 0.14	-
m_ϕ [GeV]	[0.001 - 200.0]	-	-	0.056	-
G_F		1.166379×10^{-5}		1.166649×10^{-5}	
χ_{min}^2		13.99		13.60	

Table 1. Results of the SM and SI ν fit (flavour-universal case) to the electroweak precision observables. The first column indicates the parameters, with the blocks representing the input (floating in the fit) parameters, W -boson-observables, Z -boson pole observables, and the new physics parameters (also floating in the fit within their specified ranges), respectively. The second column indicates the experimental average values taken from PDG [55]. The third (fifth) column correspond to the SM (SI ν) fit values resulting in $\chi_{\text{min}}^2 = 13.99$ (13.60). The fourth (sixth) column correspond to the pull values: $(O_{\text{fit}} - O_{\text{meas}})/\sigma_{\text{meas}}$ in the SM (SI ν) case. (Δ) denotes rescaling due to α_s dependency.

represent 1σ deviation. The SM has in total 19 parameters out of which 5 are floating in the fit, thus leaving 14 degrees of freedom. For observables with two or more experimental values, we take the weighted average, therefore $\sin^2 \theta_{\text{eff}}^\ell(\text{Avg}) = 0.23155 \pm 0.00023$ and $A_\ell(\text{Avg}) = 0.1499 \pm 0.0018$. Performing a single global fit for the SM gives $\chi_{\text{min}}^2/n_{\text{dof}} =$

13.99/14, corresponding to a p -value, $P = 45\%$. For χ^2 distributions, P is defined as

$$P \equiv \mathcal{P}(\chi_{\min}^2, n) = \int_{\chi_{\min}^2}^{\infty} \frac{x^{n/2-1} e^{-x/2} dx}{2^{n/2} \Gamma(n/2)}, \quad (3.4)$$

and Γ denotes the gamma function. This quantity is an indicator of the quality of the best fit point. The fit values and pulls are shown in the third and fourth columns of Table 1. Overall, the SM predictions fit the data extremely well, except for 2σ level tensions in A_ℓ (SLD) and A_{FB}^b .

3.2 Global Fit for the Self-interacting Neutrino Scenario

Next, we spell out our global analysis for the self-interacting neutrino model with neutrinophilic scalars. For the simplified model Eq. (1.1), three more parameters are present in addition to those in the SM,

$$\{\lambda, m_\phi, M\}. \quad (3.5)$$

We will hold M fixed around TeV, and allow the other two parameters to vary freely in the following windows, $\lambda \in [0.01, 1]$ and $m_\phi \in [0.001, 100]$ GeV. In order to directly compare with the results in the UV complete model to be discussed in the next section, we set $c_Z = -11/2$, $c_W = -2$ in Eq. (2.2). We take into account the modification to G_F due to $\Delta r^{\text{SI}\nu}$ which further shifts $m_W, \sin^2 \theta_W$ and the corresponding electroweak observables as explained in sections 2.1 – 2.4. We also include Eqs (2.18), (2.19) and (2.24), (2.25), which are direct contributions to W and Z partial decay rates into neutrino final states. Results of the global fit are presented as upper bound on λ as a function of m_ϕ , the gray excluded regions in Fig. 1. They serve as a main result of this work.

3.2.1 Flavor-Universal Case

Let us look into the flavour-universal case of neutrino self-interaction, with

$$\lambda \equiv \lambda_{ee} = \lambda_{\mu\mu} = \lambda_{\tau\tau}, \quad (3.6)$$

which has been the most popular benchmark model used for cosmological analyses [1, 3, 4, 8]. In this case, the coupling receives the strongest constraint among the flavor scenarios we consider. We perform a 2D scan in the λ versus m_ϕ parameter space. The global fit excludes the blue shaded region in the left panel of Fig. 3, also shown as the gray shaded region in the lower-right panel of Fig. 1. The exclusion is at 2σ confidence level ($\Delta\chi^2 \leq 6.18$ for 2 new physics parameters). Remarkably, for m_ϕ below GeV scale, the coupling λ is constrained to be less than $\lesssim 0.2$. For m_ϕ above ~ 300 MeV, precision electroweak fit gives the leading

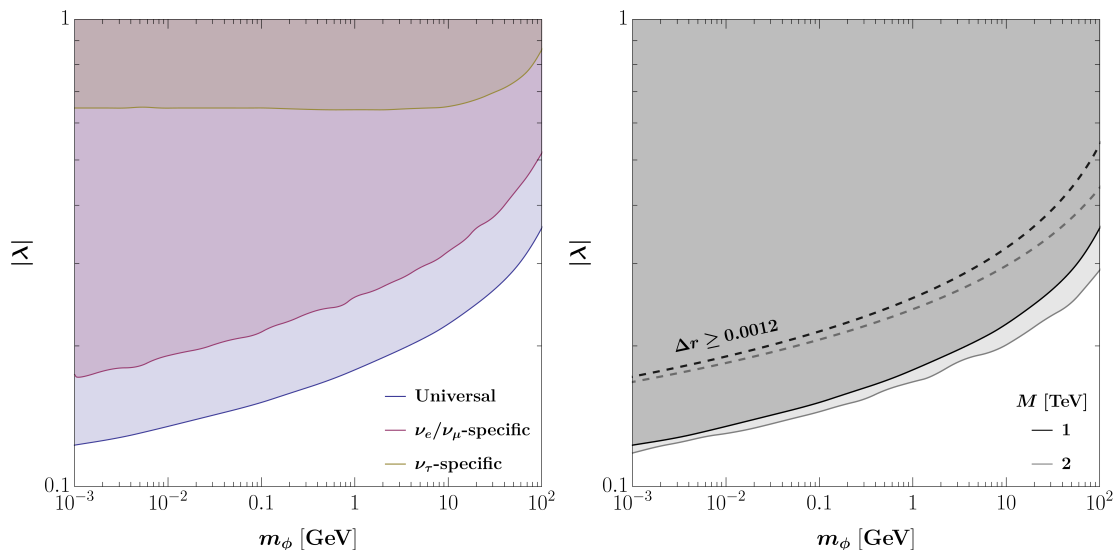


Figure 3. Precision electroweak constraints on the mass and coupling of the neutrinophilic scalar mediating neutrino self-interaction. The shaded regions are excluded at the 2σ level. *Left:* Constraints for the flavor-universal and flavor-specific cases with $M = 1$ TeV; *Right:* Flavour-universal case for two choices of M . Regions above the dashed curves denote the exclusion by requiring $|\Delta r^{\text{SI}\nu}| < 0.0012$.

constraint on λ , and it is much stronger than previously derived from Z -boson invisible width alone [29].

The right panel of Fig. 3 shows the upper bound on λ for two choices of the UV physics scale M , corresponding to the black and gray curves, respectively. The M dependence is logarithmic and mild. We also use the dashed curves to show the constraint using Eq. (2.11) which assumes neutrino self-interaction only affects the $\Delta r^{\text{SI}\nu}$ parameter. The constraint is slightly weaker which implies that the direct contributions to Z, W boson partial decay widths, albeit less important to the global fit than $\Delta r^{\text{SI}\nu}$, are not negligible.

The best fit values of parameters and observables are given in the fifth column of Table 1. It corresponds to a Fermi constant $G_F = 1.166649 \times 10^{-5} \text{ GeV}^{-2}$, which is higher than the value of G_μ in Eq. (2.7), as expected from the discussion in section 2.1. With two new parameters (λ, m_ϕ), we obtain a $\chi_{\text{min}}^2 = 13.60$, slightly lower than the SM case. In the presence of non-Gaussian priors (*i.e.*, in our scan, the new physics parameters λ and m_ϕ have flat priors in the log space), the p -value cannot be determined by evaluating $\mathcal{P}(\chi_{\text{min}}^2, n_{\text{dof}})$, and a toy Monte Carlo (MC) analysis is used. We find a higher p -value $P \simeq 54\%$ than the SM case, which implies a better goodness of fit. The improvement is rather small, thus by no means shall we claim that the self-interacting neutrino scenario is superior to the SM in the light of electroweak precision tests. A fair takeaway is, at the

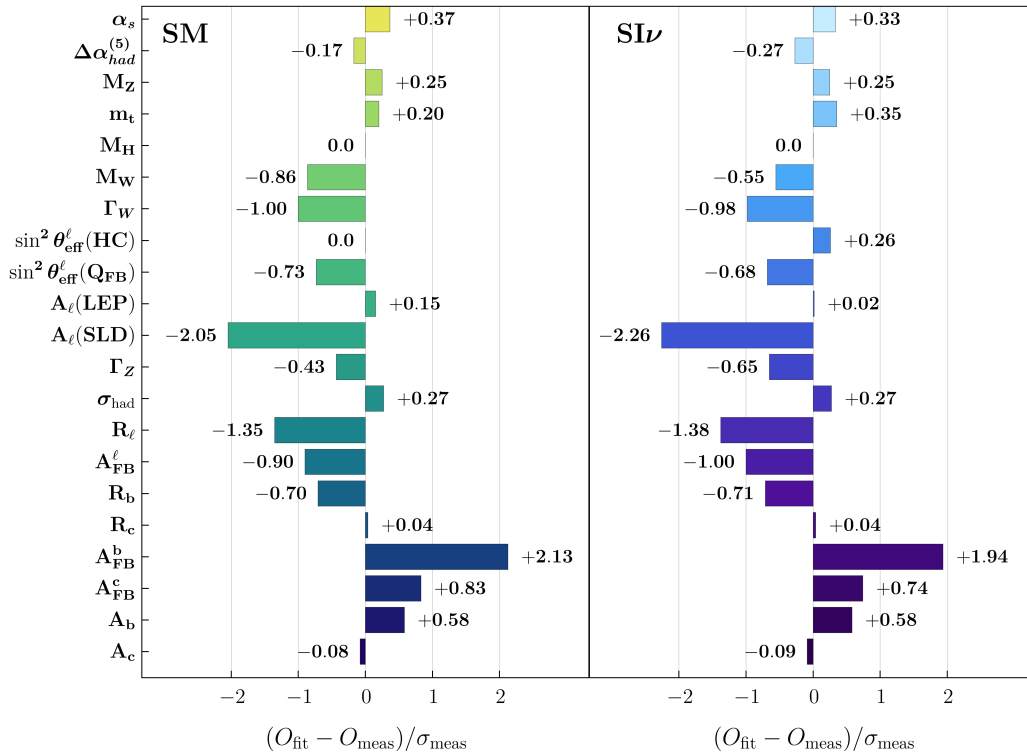


Figure 4. Pull values representing the comparison between the experimental value and fitted value for the SM (*left*) and the universal $\text{SI}\nu$ case (*right*).

best fit point, adding novel neutrino self-interaction to the SM does not make the global fit worse. The comparison of pull values in the SM and the $\text{SI}\nu$ scenario are shown in Fig. 4. In both cases, the tension with $A_\ell(\text{SLD})$ remains above 2σ , while the tension in A_{FB}^b is slightly relaxed in the $\text{SI}\nu$ case.

3.2.2 Flavor-Specific Cases

For flavor-specific cases, we turn on one coupling $\lambda \equiv \lambda_{\alpha\alpha}$ ($\alpha = e, \mu, \tau$) at a time. We perform similar analyses as the flavor-universal case and the corresponding upper bound on λ are shown by the purple and brown excluded regions in the left panel of Fig. 3. They are also shown Fig. 1.

For ν_e/ν_μ -specific case, the $\Delta r^{\text{SI}\nu}$ parameter is smaller by a factor of 1/2 than its counterpart in the flavor-universal case, because in Eq. (2.4), λ_{ee} and $\lambda_{\mu\mu}$ contribute democratically. Meanwhile, the direct shift to W/Z to neutrino decay widths is smaller by a factor of 1/3 because in Eqs. (2.18), (2.19), (2.24) and (2.25), all the three couplings contribute democratically. These suppression factors lead to a slightly weaker limit on λ from the electroweak fit than the flavor-universal case. Our global analysis finds $\chi_{\min}^2 \simeq 13.63$; $\mathcal{P} \simeq 52\%$

with the best fit value of $\lambda \sim 0.09$.

For ν_τ -specific case, $\Delta r^{\text{SI}\nu} = 0$ and there is no shift to the Fermi constant. The only impact of neutrino self-interaction occurs through the direct shift to W/Z to neutrino decay widths. From Table 1, one can see that the W width is much less precisely measured than the Z width, by a factor of ~ 10 , thus the shift to Γ_Z carries a much higher weight in the global fit. The upper limit on $\lambda_{\tau\tau}$ shown in Fig. 3 (brown shaded region) is similar to the invisible Z width constraint found before [29]. The global fit renders $\chi_{\text{min}}^2 = 13.54$ and $\mathcal{P} = 54\%$.

As an important message from Fig. 3, the upper limit on $\lambda_{\tau\tau}$ is much weaker than those on $\lambda_{ee}, \lambda_{\mu\mu}$, and λ in the flavor universal case. This comparison reveals the important role of the $\Delta r^{\text{SI}\nu}$ parameter in setting the stronger limit on λ for the latter cases.

4 Complementary Constraints

In this section, we review the other constraints on the neutrinophilic scalar parameter space that is complementary to the precision electroweak constraint derived above. As shown in Fig. 1, some of these constraints are flavor dependent and more important for small ϕ masses.

First of all, with a coupling $\lambda \gtrsim 10^{-8}$, the ϕ particles will thermalize with the SM neutrinos in the early universe. This sets a lower bound on m_ϕ to avoid excessive contribution to the radiation energy density (ΔN_{eff}) around the time of the big-bang nucleosynthesis (BBN) [56]. For ϕ as a complex scalar, the mass lower bound is about 6 MeV [57]. The magenta regions are excluded in Fig. 1.

A sufficiently light neutrinophilic scalar ϕ can be radiated by the final state neutrino in the regular leptonic decay of charged mesons $\mathbf{m}^+ = \pi^+, K^+$, leading to exotic three-body decay channels. These constraints have been explored and revisited in the literature [19, 49, 58–61]. Experimental upper bounds on $\mathbf{m}^+ \rightarrow \ell_\alpha^+ \nu_\alpha X$ (here $X = \phi$ and $\alpha = e, \mu$) have recently been set by PIENU [26], NA62 [27] (see also [62]). With a bit more details, the branching ratio of $\mathbf{m}^+ \rightarrow \ell_\alpha^+ \bar{\nu}_\alpha \phi$ is given by [61]

$$\frac{\text{Br}(\mathbf{m}^+ \rightarrow \ell_\alpha^+ \bar{\nu}_\alpha \phi)}{\text{Br}(\mathbf{m}^+ \rightarrow \ell_\alpha^+ \nu_\alpha)} = \int_{2\sqrt{\delta_\ell}}^{1+\delta_\ell-\delta_\phi} dx_\ell \frac{|\lambda_{\alpha\alpha}|^2 \sqrt{x_\ell^2 - 4\delta_\ell} [(x_\ell - 1)x_\ell - 2\delta_\ell] (\delta_\phi - \delta_\ell + x_\ell - 1)^2}{32\pi^2 \delta_\ell (\delta_\ell - 1)^2 (-\delta_\ell + x_\ell - 1)^3}, \quad (4.1)$$

where $\delta_\ell = m_{\ell_\alpha}^2/m_{\mathbf{m}}^2$, $\delta_\phi = m_\phi^2/m_{\mathbf{m}}^2$, and $x_\ell = 2E_\ell/m_{\mathbf{m}}$ with E_ℓ being the final state charged lepton energy in the rest frame of \mathbf{m} . The x_ℓ integral can be done numerically. $\text{Br}(\mathbf{m}^+ \rightarrow \ell_\alpha^+ \nu_\alpha)$ is the regular leptonic decay branching ratio measured experimentally. In Eq. (4.1), the dependence on meson decay constants (f_π, f_K , whose values are subject to

large theoretical uncertainties [63]) and the CKM matrix elements (V_{ud} , V_{us}), nicely cancel away, allowing robust upper bound on λ to be set as a function of m_ϕ . They exclude the orange and blue regions in Fig. 1. The NA62 bound was set for m_ϕ above 10 MeV [27]; We simply extrapolate it down to 6 MeV where the BBN constraint takes over.

The above meson decay constraints apply for λ_{ee} , $\lambda_{\mu\mu}$ and the flavor-universal cases, but not for $\lambda_{\tau\tau}$. In the latter case, there are two useful constraints other than BBN. One is derived based on the IceCube measurement of the spectrum of ultra-high energy astrophysical neutrinos and excludes their strong resonant scattering with the cosmic neutrino background [28]. This excludes the brown region in the lower-left panel of Fig. 1. The other constraint arises from the breaking of lepton flavor universality in Z -mediated neutrino-matter interaction which affects the global fit to neutrino oscillation data [29, 64] and excludes the red shaded region in lower left panel of Fig. 1.

The precision electroweak and neutrino oscillation constraints have a mild, logarithmic dependence on the heavy mass scale M . In Fig. 1, we set $M = 1$ TeV. In this case, the precision electroweak fit explored in this work gives the leading constraint for $m_\phi \gtrsim 300$ MeV in the case of ν_e, ν_μ -specific and the flavor universal neutrino self-interaction, and for $m_\phi \gtrsim 1$ GeV in the ν_τ -specific case.

5 Precision Electroweak Constraint on a UV Completion

In this section, we discuss a concrete UV completion that can accommodate the light neutrinophilic ϕ in Eq. (1.1). This is by extending the SM with a complex scalar T that transforms as a $SU(2)_L$ triplet and carries hypercharge -2 ,

$$T = \begin{pmatrix} T^-/\sqrt{2} & T^0 \\ T^{--} & -T^-/\sqrt{2} \end{pmatrix}. \quad (5.1)$$

The new physics part of the Lagrangian is given by

$$\begin{aligned} \mathcal{L} = & \text{Tr}[(D^\mu T)^\dagger(D_\mu T)] - M^2\text{Tr}[T^\dagger T] + \partial^\mu \phi^\dagger \partial_\mu \phi - \mu_\phi^2 |\phi|^2 \\ & - \sum_{\alpha, \beta=e, \mu, \tau} \frac{y_{\alpha\beta}}{2} \bar{L}_\alpha T i\sigma_2 L_\beta^c - y' H^T i\sigma_2 T H \phi^* + \text{h.c.} . \end{aligned} \quad (5.2)$$

The covariant derivative of T is given by $D_\mu T \equiv \partial_\mu T + i(g/2)W_\mu^a[\sigma_a, T] - ig'B_\mu T$ [65], where W_μ and B_μ are the $SU(2)_L$ and $U(1)_Y$ gauge bosons, respectively. The neutral component of the triplet T^0 only couples to neutrinos via the Yukawa interaction in the second line. However, it also carries electroweak charge and couples to the Z boson and cannot have a mass well below the weak scale. In order for the model to accommodate a light mediator for neutrino self-interaction, we also introduce a gauge-singlet complex scalar ϕ .

The presence of T is similar to Type-II seesaw mechanism for neutrino masses [66–70], however, we assume that neither T or ϕ gets a VEV, keeping the focus only on neutrino self-interactions. The nonzero neutrino mass will be explained by other sources, for example, Dirac masses as discussed in [19]. A mixing between the electric neutral scalars ϕ and T^0 is generated after spontaneous electroweak symmetry breaking, i.e., $\langle H \rangle = (0, v/\sqrt{2})^T$ with $v = 246$ GeV. The mass-mixing matrix in the basis $\{\phi, T^0\}$ can be written as

$$\mathcal{M}^2 = \begin{pmatrix} \mu_\phi^2 & y'v^2/2 \\ y'^*v^2/2 & M^2 \end{pmatrix}, \quad (5.3)$$

where μ_ϕ^2 corresponds to the mass parameter for ϕ . We are free to redefine the ϕ field to absorb the phase of the y' parameter. The mass eigenstates $\hat{\phi}$ and \hat{T}^0 can be obtained upon diagonalization of Eq. (5.3)

$$\hat{\mathbf{m}}^2 \equiv \text{diag}(m_{\hat{\phi}}^2, m_{\hat{T}^0}^2) = \mathbf{R}^T \mathcal{M}^2 \mathbf{R}, \quad (5.4)$$

where \mathbf{R} is the diagonalizing matrix characterized by a Euler angle θ , which satisfies the relation

$$\tan(2\theta) = \frac{|y'|v^2}{M^2 - \mu_\phi^2}. \quad (5.5)$$

We will work in the large M limit where

$$\sin \theta \simeq \frac{|y'|v^2}{2M^2} \simeq 0.03|y'| \left(\frac{1 \text{ TeV}}{M} \right)^2. \quad (5.6)$$

and the scalar masses eigenvalues are

$$m_{\hat{\phi}}^2 = \mu_\phi^2 - \frac{|y'|^2 v^4}{4M^2}, \quad m_{\hat{T}^0}^2 \simeq M^2 + \frac{|y'|^2 v^4}{4M^2}. \quad (5.7)$$

For simplicity, we will ignore the hat over the physical fields for the rest of the paper. It is interesting to note that the above scalar mixing lifts the mass of T^0 , allowing it to be heavier than the T^-, T^{--} partners from the triplet. However, such a mass splitting, $\delta m = \sqrt{M^2 + |y'|^2 v^4 / (4M^2)} - M$, is rather small. Even for order one $|y'|$, $\delta m \lesssim 1$ GeV, which is not of phenomenological relevance for this study. We neglect it hereafter. On the other hand, the triplet component masses can be made different by a scalar potential term, $\beta H^\dagger T T^\dagger H$ [71]

$$m_{T^-}^2 - m_{T^{--}}^2 = m_{T^0}^2 - m_{T^-}^2 = \frac{1}{4}\beta v^2. \quad (5.8)$$

The mass squares receive equal splitting. Without loss of generality, we write

$$m_{T^-} = M, \quad m_{T^0} = M + \Delta M, \quad m_{T^{--}} = \sqrt{M^2 - 2M\Delta M - (\Delta M)^2}. \quad (5.9)$$

The ϕ - T^0 mixing allows ϕ to participate in interactions with the SM sector. Essentially, for every interacting vertex involving a T^0 in the $\theta = 0$ limit, it should now be replaced by the linear combination ($T^0 \cos \theta + \phi \sin \theta$). As a result, ϕ inherits all the T^0 interactions but with couplings suppressed by a universal factor $\sin \theta$. In particular, the Yukawa coupling in Eq. (1.1) is related to the fundamental coupling y via ⁴

$$\lambda_{\alpha\beta} \simeq y_{\alpha\beta} \sin \theta. \quad (5.10)$$

ϕ also obtains $\sin \theta$ -suppressed gauge couplings from T^0 . Meanwhile, the Yukawa and gauge couplings of the physical T^0 after the mixing are rescaled by a factor of $\cos \theta$.

5.1 Tree-level $Z \rightarrow \phi\phi^*$ Decay

An immediate consequence of the ϕ - T^0 mixing is a new tree-level decay mode of the Z boson into $\phi\phi^*$, which is kinematically allowed for $m_\phi < m_Z/2$. The decay rate is

$$\Gamma_{Z \rightarrow \phi\phi^*} = \frac{\sqrt{2}G_F m_Z^3 \sin^4 \theta}{12\pi} \left(1 - \frac{4m_\phi^2}{m_Z^2}\right)^{3/2}, \quad (5.11)$$

and the final state ϕ 's will further decay into neutrinos. Although this is a $\sin^4 \theta$ order quantity, we find it to be numerically important. In [29], an upper bound $|\sin \theta| < 0.3$ was obtained by requiring $\Gamma_{Z \rightarrow \phi\phi^*} < 3 \text{ MeV}$ [55]. In the global analysis of this work, we will add this decay width to the total Z width in Eq. (2.16). In contrast, we neglect the three-body decay mode $Z \rightarrow \nu\nu\phi^*$ which can take place via off-shell T^0 but is phase space suppressed and subdominant.

5.2 Structure of Radiative Corrections to $\delta g_Z, \delta g_W$

Moving on to loops, we first clarify the structure of radiative corrections to the neutrino gauge couplings $\delta g_Z, \delta g_W$ in this UV complete model and their relationship with those derived in the simplified model in Eq. (2.2). In the presence of the mixing, both ϕ and T contribute at one-loop level, through the gauge vertex and self-energy diagrams. The finiteness of $\delta g_Z, \delta g_W$ is guaranteed by gauge invariance and the Ward identity. We leave the discussion of gauge boson vacuum polarization diagrams in section 5.5, which contribute as the electroweak oblique parameters at energy scales well below the triplet mass.

In general, the correction to δg_V ($V = Z, W$) can be written as

$$\delta g_V = (\delta g_V)_\phi + (\delta g_V)_T, \quad (5.12)$$

⁴The doubly-charged component T^{--} only couples to a pair of charged leptons. As mentioned in the paragraph below Eq. (2.3), we assume y to be flavor diagonal, $y_{\alpha\beta} = 0$ for $\alpha \neq \beta$. This choice forbids the dangerous lepton flavor changing decays mediated by T^{--} [72].

where $(\delta g_V)_\phi$ receives contributions from loop diagrams that contain at least one ϕ . It occurs at $\sin^2 \theta$ order or higher. In contrast, $(\delta g_V)_T$ is from diagrams with only the triplet T in the loop.

It is useful to reorganize Eq. (5.12) as the following

$$\begin{aligned} \delta g_V &= (\delta g_V)_\phi + \left[(\delta g_V)_T - (\delta g_V)_{T, \theta=0} \right] \\ &+ (\delta g_V)_{T, \theta=0} . \end{aligned} \quad (5.13)$$

The quantity in the square bracket is nonzero due to the different Yukawa and gauge couplings of T in the $\theta \neq 0$ and $\theta = 0$ cases. It is also of $\sin^2 \theta$ order or higher.

The second line of Eq. (5.13) represents the contribution of T in the absence of $\phi - T^0$ mixing whose finiteness is another consequence of gauge invariance. As a result, both lines of Eq. (5.13) are free from UV divergences.

The first line of Eq. (5.13) has already been carefully calculated in [29] and the results are given by Eq. (2.2) with $c_Z = -11/2$ and $c_W = -2$. Up to a loop factor, this contribution is of order

$$\lambda^2 \ln \frac{M^2}{m_\phi^2} \sim \frac{y^2 y'^2 v^4}{M^4} \ln \frac{M^2}{m_\phi^2} , \quad (5.14)$$

where in the second step we used Eqs. (5.6) and (5.10). In comparison, the second line of Eq. (5.13) corresponds to the radiative correction from T in the absence of ϕ field. It will be calculated in the next section and the contributions are of order

$$\frac{y^2 q^2}{M^2} , \quad (5.15)$$

where the logarithmic factor is absent.

As we already see in Figs. 1 and 3, the precision electroweak constraints are sensitive to $\lambda \gtrsim 0.1$. This corresponds to the triplet mass M around TeV scale. For sufficiently small m_ϕ , the logarithmic factor is large allowing the first line of Eq. (5.13) to be important, which has been explored in [29]. On the other hand, the prefactor in front of the log is suppressed compared to Eq. (5.15) by an extra M^2 . This implies that the heavy T contribution cannot be simply ignored for Z -pole physics where $q^2 = m_Z^2$. The competition is between $\sin^2 \theta \cdot \ln(M^2/m_\phi^2)$ and $(m_Z/M)^2$.

5.3 Heavy T contribution to δg_Z , δg_W and $Z\ell^+\ell^-$ Couplings

In this work, we complete the calculation of [29] by including the second line of Eq. (5.13), *i.e.*, radiative correction to gauge couplings from the heavy triplet T . As already discussed, this contribution occurs in $\theta = 0$ limit.

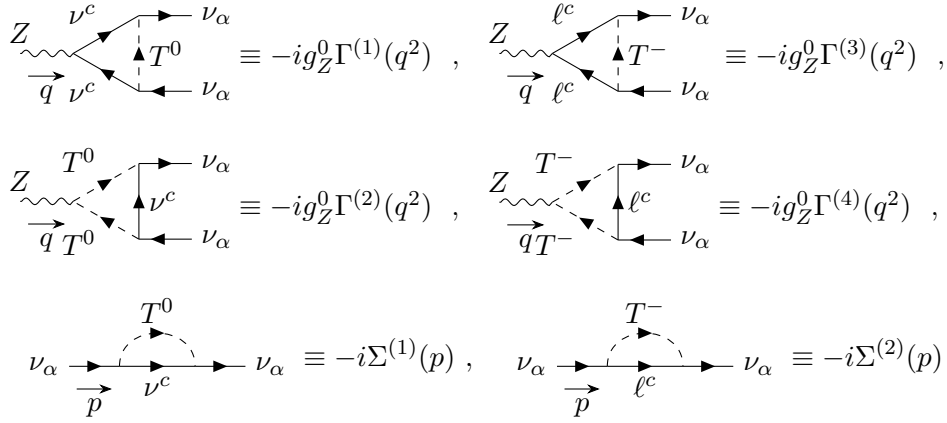


Figure 5. One-loop vertex and self-energy corrections to the $Z\nu\bar{\nu}$ vertex due to the heavy scalars T^0 and T^- .

We first calculate the correction to the $Z\nu\bar{\nu}$ coupling, g_Z defined in Eq. (2.1). The relevant Feynman diagrams are shown in Fig. 5. Assuming flavor diagonal Yukawa couplings, $y_{\alpha\beta} = y_{\alpha\alpha}\delta_{\alpha\beta}$, the corresponding loop functions are

$$\begin{aligned}
\Gamma^{(1)} &= -\frac{|y_{\alpha\alpha}|^2}{32\pi^2} \left[\frac{2}{\varepsilon} - 1 + f_1(q^2, M, \mu) \right], & \Gamma^{(3)} &= \frac{1}{2}(-1 + 2\sin^2\theta_W)\Gamma^{(1)}, \\
\Gamma^{(2)} &= \frac{|y_{\alpha\alpha}|^2}{16\pi^2} \left[\frac{2}{\varepsilon} + f_2(q^2, M, \mu) \right], & \Gamma^{(4)} &= \frac{1}{2}\sin^2\theta_W\Gamma^{(2)}, \\
\Sigma^{(1)} &= -\frac{|y_{\alpha\alpha}|^2}{32\pi^2} \left(\frac{2}{\varepsilon} + \frac{1}{2} + \log\frac{\mu^2}{M^2} \right) \not{p}, & \Sigma^{(2)} &= \frac{1}{2}\Sigma^{(1)},
\end{aligned} \tag{5.16}$$

where μ is the renormalization scale and the loop function f_1 has been defined in Eq. (2.3) and f_2 is given by

$$f_2(q^2, M, \mu) = 2 \int_0^1 dx \int_0^{1-x} dy \ln \frac{\mu^2}{(x+y)M^2 - xyq^2} \tag{5.17}$$

Their correction to g_Z is

$$\left. \frac{(\delta g_Z)_{\alpha\alpha}}{g_Z^0} \right|_{T, \theta=0} = \sum_{i=1}^4 \Gamma^{(i)} + \sum_{j=1}^2 \frac{\partial \Sigma^{(j)}}{\partial \not{p}}. \tag{5.18}$$

All the $1/\varepsilon$ divergences and the $\ln\mu$ dependence cancel away in the sum, as expected. In the large M limit, Eq. (5.18) vanishes as q^2/M^2 , which verifies the decoupling theorem. We add the heavy T contribution as part of δg_Z in Eq. (2.18).

The heavy triplet loop can also give correction to the coupling between the Z boson and left-handed charged leptons. The neutral-current interacting Lagrangian for charged

leptons is

$$\begin{aligned}\mathcal{L} &= -g_Z^0 \bar{\ell}_\alpha \gamma^\mu (g_{V,\ell_\alpha} - g_{A,\ell_\alpha} \gamma_5) \ell_\alpha Z_\mu \\ &= -g_Z^0 \bar{\ell}_\alpha \gamma^\mu \left[-\sqrt{\rho_Z^{\ell_\alpha}} \mathbb{P}_L + 2\sqrt{\rho_Z^{\ell_\alpha} \kappa_Z^{\ell_\alpha}} \sin^2 \theta_W (\mathbb{P}_L + \mathbb{P}_R) \right] \ell_\alpha Z_\mu ,\end{aligned}\quad (5.19)$$

where we used Eq. (2.13) and $\ell_\alpha = e^-, \mu^-, \tau^-$. Because the right-handed current is not affected by T , the radiative correction must keep the product $\sqrt{\rho_Z^{\ell_\alpha} \kappa_Z^{\ell_\alpha}}$ intact, which implies

$$\left(\sqrt{\rho_Z^{\ell_\alpha}} - 1 \right)_{T,\theta=0} \simeq - \left(\kappa_Z^{\ell_\alpha} - 1 \right)_{T,\theta=0} . \quad (5.20)$$

Only the first term in the square bracket in Eq. (5.19), which is proportional to the weak isospin, is affected by T loops. The corresponding Feynman diagrams are shown in Fig. 6. These loop functions have the same structure as those in Eq. (5.16), up to different couplings

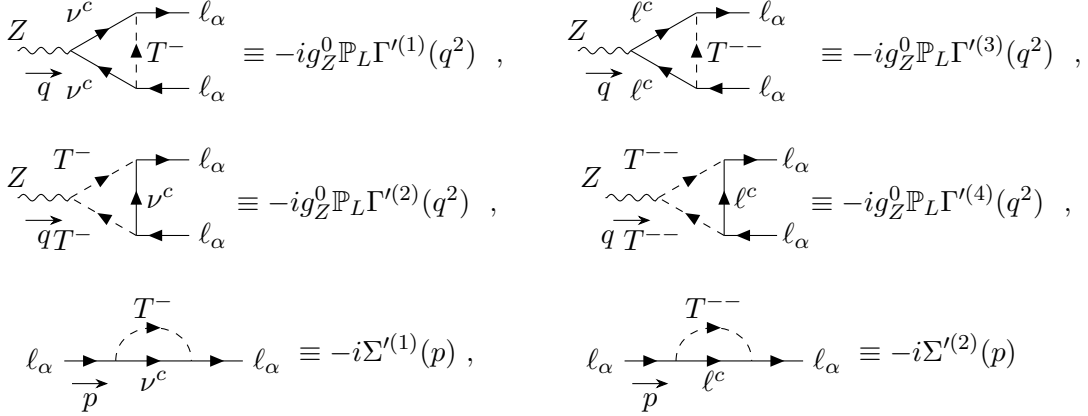


Figure 6. One-loop vertex and self-energy corrections to the $Z\ell^+\ell^-$ coupling due to heavy scalars T^- and T^{--} . The prime does not mean derivative.

at vertices,

$$\begin{aligned}\Gamma'^{(1)} &= \frac{1}{2}\Gamma^{(1)}, \quad \Gamma'^{(2)} = \frac{1}{2}\sin^2 \theta_W \Gamma^{(2)}, \quad \Sigma'^{(1)} = \Sigma^{(2)} = \frac{1}{2}\Sigma^{(1)}, \\ \Gamma'^{(3)} &= (-1 + 2\sin^2 \theta_W)\Gamma^{(1)}, \quad \Gamma'^{(4)} = (-1 + 2\sin^2 \theta_W)\Gamma^{(2)}, \quad \Sigma'^{(2)} = \Sigma^{(1)} .\end{aligned}\quad (5.21)$$

The resulting shift to the electroweak form factor is

$$\left(\sqrt{\rho_Z^{\ell_\alpha}} - 1 \right)_{T,\theta=0} = - \left[\sum_{i=1}^4 \Gamma'^{(i)} + (-1 + 2\sin^2 \theta_W) \sum_{j=1}^2 \frac{\partial \Sigma'^{(j)}}{\partial \not{p}} \right] . \quad (5.22)$$

Again, the result is UV finite. The shift in $\sqrt{\rho_Z^{\ell_\alpha}}$ and $\kappa_Z^{\ell_\alpha}$ affect both the asymmetry parameters and the Z -boson partial decay width, and in turn other electroweak observables,

as discussed in section 2.3. Both Eqs. (5.18) and (5.22) are contributions from heavy T to Z -pole physics, thus they are evaluated at momentum transfer $q^2 = m_Z^2$.

Finally, we calculate the correction to the $W\ell\bar{\nu}$ coupling, g_W defined in Eq. (2.1). The vertex Feynman diagrams are shown in Fig. 7. We do not show the self-energy diagrams which are identical to those in Figs. 5 and 6. The loop functions are equal to

$$\begin{aligned} & \text{Diagram 1: } W^- \text{ (wavy, } q \text{)} \text{ and } \nu^c \text{ (solid) enter from bottom. } T^- \text{ (dashed) loop connects } W^- \text{ and } \nu^c. \text{ } \ell^-_\alpha \text{ (solid) and } \nu_\alpha \text{ (solid) exit to the right.} \\ & \text{Diagram 2: } W^- \text{ (wavy, } q \text{)} \text{ and } \nu^c \text{ (solid) enter from bottom. } T^- \text{ (dashed) loop connects } W^- \text{ and } \ell^c \text{ (solid).} \\ & \text{Diagram 3: } W^- \text{ (wavy, } q \text{)} \text{ and } \nu^c \text{ (solid) enter from bottom. } T^{--} \text{ (dashed) loop connects } W^- \text{ and } \ell^c \text{ (solid).} \end{aligned}$$

$$\begin{aligned} & \equiv -ig_W^0 \Gamma''^{(1)}(q^2) \ , \\ & \equiv -ig_W^0 \Gamma''^{(2)}(q^2) \ , \quad \equiv -ig_W^0 \Gamma''^{(3)}(q^2) \ , \end{aligned}$$

Figure 7. One-loop vertex and self-energy corrections to the $W\ell\bar{\nu}$ vertex due to the heavy scalars.

$$\Gamma''^{(1)} = \frac{1}{2}\Gamma^{(1)}, \quad \Gamma''^{(2)} = \Gamma''^{(3)} = \frac{1}{2}\Gamma^{(2)}. \quad (5.23)$$

The finite correction to g_W is given by

$$\left. \frac{(\delta g_W)_{\alpha\alpha}}{g_W^0} \right|_{T, \theta=0} = \sum_{i=1}^3 \Gamma''^{(i)} + \frac{1}{2} \sum_{j=1}^2 \frac{\partial \Sigma^{(j)}}{\partial \not{p}} + \frac{1}{2} \sum_{j=1}^2 \frac{\partial \Sigma'^{(j)}}{\partial \not{p}}. \quad (5.24)$$

The radiative correction to $W\ell\bar{\nu}$ coupling from T depends on the momentum transfer of a specific charged-current process through the ratio q^2/M^2 . It vanishes in the $M \rightarrow \infty$ limit as required by the decoupling theorem. The correction is suppressed by q^2 for low-energy processes such as weak decays.⁵ For electroweak observables, its effect is strongest in W -boson decay where $q^2 = m_W^2$. We include the heavy T contribution as part of δg_W in Eq. (2.24). In contrast, the effect is negligible in muon decay and the corresponding Δr parameter because $q^2 < m_\mu^2$. In the UV complete model, the contribution to Δr remains the same as Eq. (2.4).

In section 5.2, we have discussed the parametrical dependence of radiative corrections to δg_V ($V = Z, W$) from the light ϕ and heavy T contributions. Now with the concrete calculations, we are able to make a more precise comparison and highlight the interplay of parameters in the UV complete model.

The above T induced radiative corrections are all proportional to the fundamental Yukawa coupling y^2 . Using Eq. (5.10), for fixed λ , $y = \lambda/\sin\theta$ is inversely proportional to

⁵The same is true for the heavy T contributions to δg_W , δg_Z , and the $Z\ell^+\ell^-$ couplings.

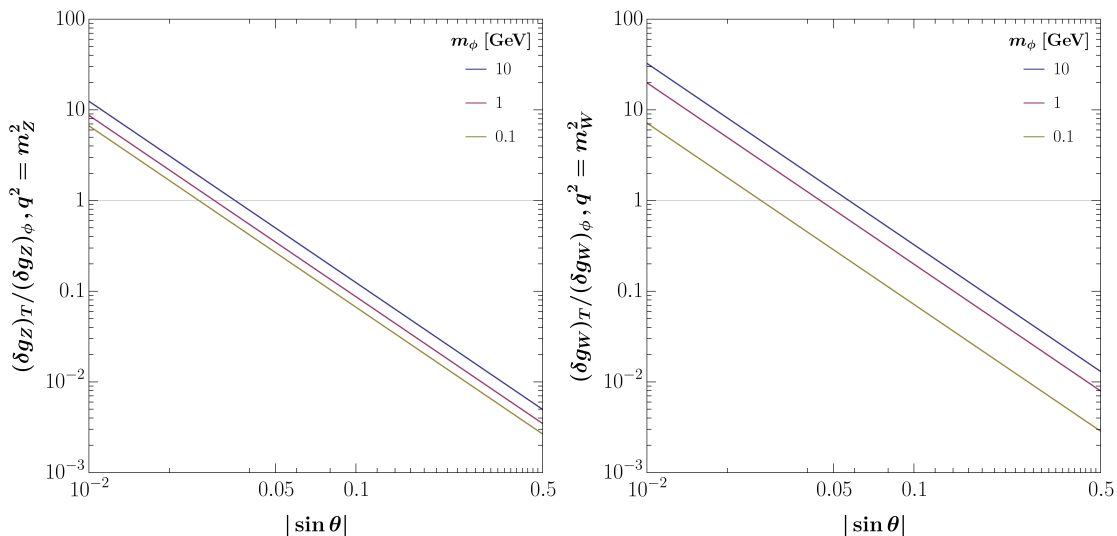


Figure 8. Ratio of the heavy T versus light ϕ contribution to $\delta g_{Z,W}$, with respect to $\sin \theta$ for three different choice of m_ϕ , and $M = 1$ TeV. The heavy T contribution is negligible for $\sin \theta \gtrsim 0.05$.

the mixing parameter $\sin \theta$. As a result, the T contribution can be subdominant to that of ϕ for sufficiently large $\sin \theta$. In Fig. 8, we show the ratio of heavy T contribution to $\delta g_{Z,W}$ derived in Eqs. (5.18) and (5.24) to the light ϕ contribution given in Eq. (2.2) as a function of $\sin \theta$ for several choices of m_ϕ . We hold $M = 1$ TeV fixed. The coupling λ dependence cancels away in this ratio. We find that the ratio is smaller than 1 for $|\sin \theta| \gtrsim 0.05$. This is the parameter space where the light ϕ contribution dominates the radiative corrections and the precision electroweak constraints shown in Fig. 1 continue to hold in the UV complete model. We also note that for light ϕ below half of the Z mass, $|\sin \theta|$ cannot be made too large due to the $Z \rightarrow \phi\phi^*$ constraint discussed in section 5.1. The value of $|\sin \theta|$ is further bounded from above due to the unitarity constraint on $|y'|$.⁶

In the above results, Eqs. (5.18), (5.22) and (5.24), a small mass splitting among the triplet components, ΔM , has been neglected. This amounts to neglecting terms suppressed by $\Delta M/M \ll 1$. The mass splitting plays a more important role in the contribution to electroweak oblique parameters, as will be discussed in section 5.5.

5.4 Constraints from Global Fit

Here we discuss the procedure of precision electroweak fit in the UV complete model with the $SU(2)_L$ scalar triplet. Compared to the simplified model explored in section 3, the UV completion has two additional parameters. The complete set of beyond SM parameters are

$$\{\lambda, m_\phi, \sin \theta, M, \Delta M\}. \quad (5.25)$$

⁶Using Eq. (5.6) and requiring $|y'| < 4\pi$, we obtain $|\sin \theta| < 0.38 (1 \text{ TeV}/M)^2$.

To reduce number of parameters in the scanning, we make two simplifications to our analysis. First, the LHC experiment already constrains the doubly-charged scalar mass to be above ~ 900 GeV [73–75]. Meanwhile, the precision electroweak fit is sensitive to $\lambda, \sin \theta \sim \mathcal{O}(0.1)$, which corresponds to M not far above TeV scale, through Eqs. (5.6) and (5.10). Thus we hold $M = 1$ TeV fixed in the analysis. Furthermore, as will be discussed in section 5.5, the mass splitting parameter ΔM mainly controls the oblique parameter T and is strongly correlated to m_ϕ and $\sin \theta$. We do not include the heavy triplet contribution to S, T, U in the global fit. Instead, their ranges are determined posteriorly from the fit, which is then used to solve for ΔM consistent with the oblique constraints. These considerations help to reduce the free parameters of scanning down to three

$$\{\lambda, m_\phi, \sin \theta\} . \quad (5.26)$$

The parameter ranges of our scan are

$$\lambda \in (10^{-2}, 1), \quad \sin \theta \in (10^{-2}, 1), \quad m_\phi \in (10^{-3}, 10^2) \text{ GeV} . \quad (5.27)$$

The results are shown in Fig. 9. We focus on case where T and ϕ couple universally to the three neutrino flavors. Similar results hold for flavor specific cases. In the left panel, the purple shaded region is excluded at 2σ level in the λ versus m_ϕ parameter space where we allow $\sin \theta$ to float in the scan. This corresponds to the most conservative limit in the UV complete model. The best-fit point corresponds to $\sin \theta = 0.26$, with $\chi_{\min}^2 = 13.22$. The corresponding p -value $P = 67\%$ is determined by the toy MC analysis. In the same plot, the blue shaded region corresponds to the 2σ exclusion in the simplified model derived early on and shown as the blue shaded region in Fig. 3 (left). The very small difference between the purple and blue shaded regions implies that resorting to the UV completion does not significantly improve the global fit to the electroweak observables. Near the best fit point with $|\sin \theta| = 0.26$, it is good enough to use the simplified model to set constraint on λ versus m_ϕ .

Because the value of $\sin \theta$ is set by nature rather than by the authors, we also perform scans in the λ versus m_ϕ plane for several other choices of $\sin \theta$ equal to 0.05, 0.03, 0.02. The results are shown as the black solid, dashed and dotted lines, respectively. We find the upper bound on λ gets stronger and less m_ϕ dependent for smaller values of $\sin \theta$. This behavior is consistent with the discussions around Fig. 8. For very small $\sin \theta$, the heavy T contribution to radiative corrections is enhanced and dominates over that from light ϕ . On the other hand, for $\sin \theta \gtrsim 0.03$, ϕ dominates and the upper bound on λ is very similar to the simplified model result.

In the right panel of Fig. 9, the black dashed curve shows the precision electroweak constraint, upper bound on $|\sin \theta|$ as a function of m_ϕ , where we allow $|\lambda|$ to float between

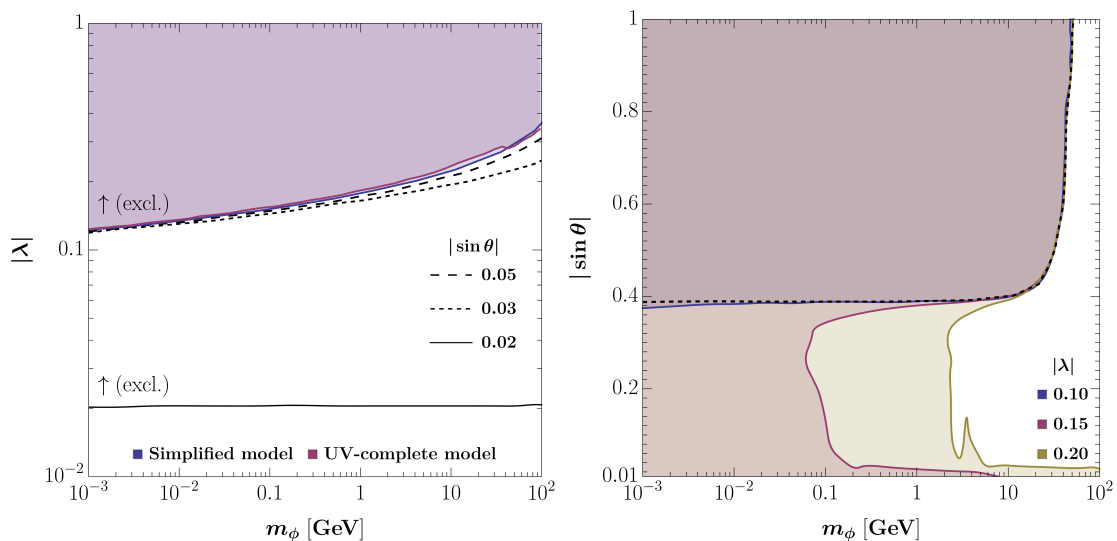


Figure 9. Constraints on the UV-complete model for the flavor-universal case. The shaded regions are excluded at the 2σ level. *Left:* The dashed, dotted and solid black curves correspond to fixed values of $|\sin\theta|$, while purple and blue shaded regions represent the results of the global analysis for the UV-complete model ($|\sin\theta| \in \{0.01, 1.0\}$) and the simplified model, respectively. *Right:* Exclusion curves in the $|\sin\theta|$ vs. m_ϕ plane for fixed values of λ . The dashed curve denotes the exclusion from the global fit where $|\lambda| \in \{0.01 - 1.0\}$.

0.01 and 1. We also use the shaded regions to show the exclusion for several cases of fixed $|\lambda|$ values. All are at 2σ level. The parameter space with $m_\phi < m_Z/2$ and $|\sin\theta| \gtrsim 0.4$ is always excluded due to too large $Z \rightarrow \phi\phi^*$ decay width, as discussed in section 5.1. For intermediate range of the mixing parameter $0.03 \lesssim |\sin\theta| \lesssim 0.4$, a larger $|\lambda|$ leads to a stronger lower bound on m_ϕ , which is consistent with the shape of exclusion curve in the left panel. For $|\lambda| = 0.15$ and 0.2 , the very small $|\sin\theta|$ region is excluded regardless of m_ϕ because of the heavy T dominance. Similar floor also exists for smaller $|\lambda| = 0.1$ but only excludes low $|\sin\theta|$ values that lie outside the plot range.

5.5 Contribution to Electroweak Oblique Parameters

Finally, we discuss the loop corrections from the triplet T through the vacuum polarization diagrams of the SM vector bosons. At energy scales higher than M , the triplet contributes to the beta functions of $SU(2)_L$ and $U(1)_Y$ gauge couplings. This does not bring additional constraint, due to the lack of precision measurements at those high energies. For momentum transfers well below the triplet mass, their remnant effects in the gauge boson self-energy diagrams are accounted for by the electroweak oblique parameters [76–78].

The oblique parameters contributed by a $SU(2)_L$ triplet scalar have been explored in

the literature [79–81]. Here, we generalize those results by introducing a light scalar ϕ and switching on its mixing with T^0 . Following the notations used in [82],

$$\begin{aligned}
S &= \frac{16\pi c^2 s^2}{e^2} \left[\frac{A_{ZZ}(M_Z) - A_{ZZ}(0)}{M_Z} - \frac{c^2 - s^2}{cs} \frac{\partial A_{\gamma Z}(P)}{\partial P} \Big|_{P=0} - \frac{\partial A_{\gamma\gamma}(P)}{\partial P} \Big|_{P=0} \right], \\
T &= \frac{4\pi}{e^2} \left[\frac{A_{WW}(0)}{M_W} - \frac{A_{ZZ}(0)}{M_Z} \right], \\
U &= \frac{16\pi s^2}{e^2} \left[\frac{A_{WW}(M_W) - A_{WW}(0)}{M_W} - c^2 \frac{A_{ZZ}(M_Z) - A_{ZZ}(0)}{M_Z} - 2cs \frac{\partial A_{\gamma Z}(P)}{\partial P} \Big|_{P=0} \right. \\
&\quad \left. - s^2 \frac{\partial A_{\gamma\gamma}(P)}{\partial P} \Big|_{P=0} \right], \tag{5.28}
\end{aligned}$$

where $s = \sin \theta_W$, and $c = \sqrt{1 - s^2}$. Here, the capital M_i 's represent the corresponding mass square, *i.e.*, $M_W = m_W^2$, $M_Z = m_Z^2$. The capital P is equal to p^2 with p^μ being the external momentum of each vector polarization diagram.

The vacuum polarization amplitudes are given by

$$\begin{aligned}
A_{\gamma\gamma}(P) &= \frac{e^2}{8\pi^2} [4F(M_{-1}, M_{-1}, P) + F(M_0, M_0, P)], \\
A_{\gamma Z}(P) &= \frac{e^2}{8\pi^2 cs} [2(c^2 - s^2)F(M_{-1}, M_{-1}, P) - s^2 F(M_0, M_0, P)], \\
A_{WW}(P) &= \frac{e^2}{8\pi s^2} \{ F(M_0, M_{-1}, P) + [\cos^2 \theta F_s(M_{+1}) + \sin^2 \theta F_s(M_\phi)] + F_s(M_0) \\
&\quad + [\cos^2 \theta F_b(M_{+1}, M_0, P) + \sin^2 \theta F_b(M_\phi, M_0, P)] \}, \\
A_{ZZ}(P) &= \frac{e^2}{8\pi^2 c^2 s^2} \{ (c^2 - s^2)^2 F(M_{-1}, M_{-1}, P) + s^4 F(M_0, M_0, P) + 2 \cos^2 \theta F_s(M_{+1}) \\
&\quad + 2 \sin^2 \theta F_s(M_\phi) + [\cos^4 \theta F_b(M_{+1}, M_{+1}, P) + 2 \sin^2 \theta \cos^2 \theta F_b(M_{+1}, M_\phi, P) \\
&\quad + \sin^4 \theta F_b(M_\phi, M_\phi, P)] \}, \tag{5.29}
\end{aligned}$$

where M_{+1}, M_0, M_{-1} denote the mass squares of the triplet components T^0, T^-, T^{--} given in Eq. (5.9), and $\sin \theta$ is the ϕ - T^0 mixing parameter introduced in Eq. (5.6). Because T^0 is electric neutral, $A_{\gamma Z}$ and $A_{\gamma\gamma}$ do not depend on M_{+1} .

The functions F_s, F_b are the finite part of the sunrise and bubble diagrams in Fig. 11,

$$F_s(M) = \frac{1}{2} M \ln M, \tag{5.30}$$

$$F_b(M_1, M_2, P) = - \int_0^1 dx [(x^2 - x)P + xM_1 + (1 - x)M_2] \ln [(x^2 - x)P + xM_1 + (1 - x)M_2],$$

and we further write

$$\begin{aligned}
F(M_1, M_2, P) &= F_s(M_1) + F_s(M_2) + F_b(M_1, M_2, P), \\
F(M, M, P) &= 2F_s(M) + F_b(M, M, P). \tag{5.31}
\end{aligned}$$

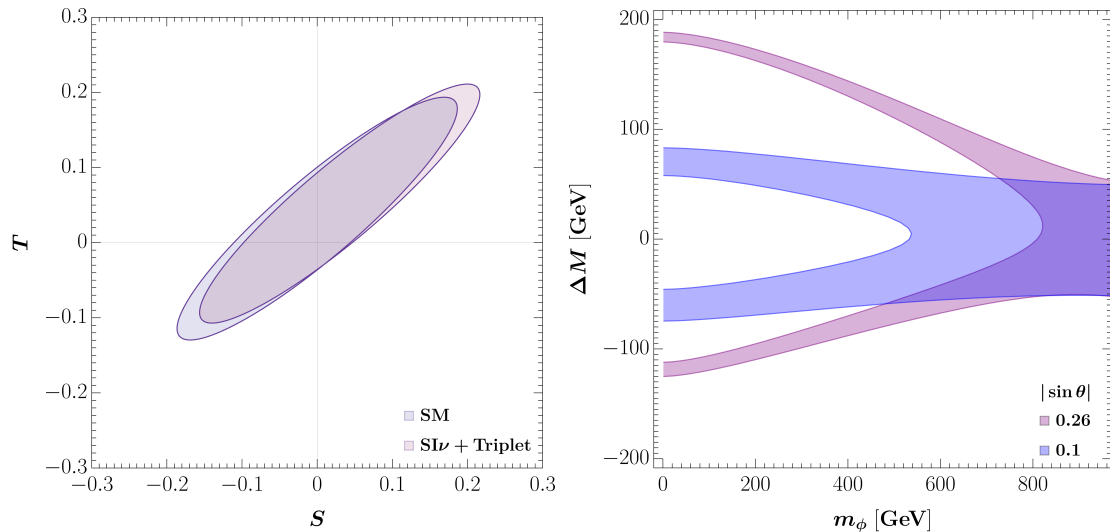


Figure 10. *Left:* Electroweak precision constraints (2σ) on S and T ($U = 0$) in the SM and the UV complete model after including all the other corrections. *Right:* Correlation between ΔM and m_ϕ for $M = 1$ TeV and two choices of $\sin\theta$. The shaded regions correspond to S, T within the ranges, $T = 0.052 \pm 0.064$ and $S = 0.03 \pm 0.075$, consistent with the purple ellipse in the left panel.

A useful identity for our calculation is

$$\left. \frac{\partial F(M, M, P)}{\partial P} \right|_{P=0} = \frac{1}{6}(1 + \ln M) . \quad (5.32)$$

The impact of S, T, U parameters on electroweak observables are listed in appendix B of [77]. In the $\theta = 0$ limit, the contribution from a triplet with degenerate masses at TeV scale is safely small given the existing constraints. This is no longer the case in the presence of T^0 mixing with a light ϕ , which contributes to custodial symmetry violation at loop level and can give a potentially large contribution to the T parameter.

The global analysis discussed earlier has taken into account the radiative corrections to the gauge-fermion couplings calculated in section 5.3 but not the oblique parameters. Instead, the allowed range of S, T, U parameters for the best fit point is obtained as a spin-off of the analysis done by `Gfitter`. The result is depicted by the purple ellipse in

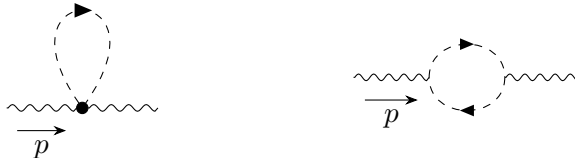


Figure 11. Sunrise and bubble diagrams for Z, W self-energy diagrams from scalar triplet.

the left panel of Fig. 10. We only show the S versus T plane because the constraint on U is much weaker. For comparison, we use the blue ellipse to show the ranges of S, T in the SM. The difference between the two ellipses is small, which is another evidence showing that self-interacting neutrino models (simplified or UV completed) does not substantially improve the electroweak global fit over the SM.

In the right panel of Fig. 10, we show the ΔM versus m_ϕ parameter space where the predictions for S, T parameters are within the purple ellipse in the left panel. We hold $M = 1 \text{ TeV}$ fixed and the blue and purple regions correspond to $\sin\theta = 0.1$ and 0.26 , respectively. For small m_ϕ , we find that a mass splitting along the triplet components ΔM of order $\pm 100 \text{ GeV}$ is needed. It is mainly driven by suppressing the T parameter. Due to the strong correlation between ΔM , m_ϕ and $\sin\theta$, we did not directly include the electroweak oblique parameters in the global fit.

As the main message from the discussions of this subsection, it is always possible to find a proper ΔM value to suppress the oblique parameters. This requires some tuning among the UV complete model parameters, and it is the price one needs to pay in order to accommodate a light ϕ that mediates strong neutrino self-interaction.

6 Conclusions and Outlook

Novel neutrino self-interaction with strength much higher than predicted by the Fermi theory continues to serve as a well-motivated candidate of new physics. Extension of the SM with a light neutrinophilic scalar ϕ has been employed as the leading model and has been the target of various probes in the laboratories and cosmology. In this work, we perform an in-depth study of one-loop radiative corrections in such a model and derive, for the first time, precision electroweak constraints on the self-interacting neutrino parameter space. Our investigation is made in both simplified model with only ϕ and a concrete UV completion with additional neutrinophilic scalars.

In the simplified model, radiative corrections to the electroweak sector can be computed with the guidance of gauge invariance restoration and the Ward identity. The general forms of neutrino neutral- and charged-current couplings (g_Z, g_W) are presented in Eq. (2.2), which features a logarithmic enhancement factor in the light ϕ limit. The presence of the log factor does not depend on the UV completion details. The correction to g_Z mainly contributes to the invisible Z decay width, whereas the correction to g_W can affect the Fermi constant measurement. The latter occurs through the Δr parameter which in turn modifies the prediction for a number of electroweak observables as detailed in section 2. We modify the public `Gfitter` code to include all the effects and perform a global fit to the most recent data from lepton and hadron colliders. The results are summarized in Fig. 1

which represent the state-of-art constraints on the neutrinophilic coupling λ as a function of m_ϕ . The precision electroweak constraints derived in this work are the leading ones for m_ϕ above a few hundred MeV scale. For the flavor universal and ν_e/ν_μ specific neutrino self-interactions, the constraints are much stronger than the previous limit derived only using the invisible Z width. This further allows us to report the highest value of G_{eff}

$$G_{\text{eff}} < \begin{cases} 1.4 \times 10^{-6} \text{ MeV}^{-2}, & \text{flavor universal case} \\ 3.5 \times 10^{-6} \text{ MeV}^{-2}, & \nu_e \text{ specific case} \\ 4.1 \times 10^{-6} \text{ MeV}^{-2}, & \nu_\mu \text{ specific case} \\ 2.3 \times 10^{-4} \text{ MeV}^{-2}, & \nu_\tau \text{ specific case} \end{cases} \quad (6.1)$$

These findings will serve as a road map for further explorations on neutrino cosmology and origin of dark matter. The correct relic abundance of sterile neutrino dark matter can be produced through the oscillation mechanism in the presence of neutrino self-interaction [9] and our precision electroweak constraints are relevant for the large and intermediate ϕ mass regions of the relic target. Our new constraints also facilitate interesting interplay with upcoming experimental searches. As an example, consider the lower-right panel of Fig. 1 for the case of flavor universal neutrino self-interaction. Currently, the largest G_{eff} is found at the intersection of PIENU and BBN constraints. If future pion decay experiments (*e.g.*, [83]) improve the sensitivity by another order of magnitude, the largest G_{eff} value will shift to the intersection of NA62 and precision electroweak constraints.

We assess the robustness of the above results by considering a concrete UV complete model which extends the SM with ϕ and an $SU(2)_L$ triplet scalar T . The mass of T lies around the TeV scale and the simplified model is obtained by integrating out the triplet. It is straightforward to calculate the radiative corrections in such a renormalizable and gauge invariant model. We compare the new corrections involving the heavy T in the loop diagrams to those in the simplified model. An important parameter that controls their relative importance is the mixing between ϕ and the electric neutral component of the triplet T^0 , which we call $\sin\theta$. For $\sin\theta \gtrsim 0.03$, we find that the light ϕ contribution dominates and the upper bound on λ shown in Fig. 1 remain intact. However, for sufficiently small values of $\sin\theta$, the triplet becomes strongly coupled and its contribution can overwhelm that of ϕ , resulting in much stronger bounds as shown in Fig. 9. Another effect of the ϕ - T^0 mixing is the potential large contribution to the electroweak oblique parameter T . We point out that it can be suppressed with a suitable choice of the triplet mass splitting parameter ΔM . These moving parts decides whether the constraints found in the simplified model apply and when the additional contributions in the UV complete model must be taken into account.

We end with a brief comment on another possible UV completion which resorts to heavy vectorlike neutrino N instead of the scalar triplet. The light scalar ϕ originally couples to N . Its neutrinophilic coupling λ in the simplified model can be generated by the mixing between N and light neutrinos. By construction, λ contains two powers of the ν - N mixing, in contrast to the single power of ϕ - T^0 mixing in the scalar triplet model. As a result, we expect stronger constraints on λ in this alternative UV completion. A detailed exploration of it is beyond the scope of the present work and will be done elsewhere.

Acknowledgments

We thank Ayres Freitas, Douglas Tuckler and Antonio Coutinho for useful discussions, and Ayres Freitas for commenting on the draft. DV acknowledges support from the Canada First Research Excellence Fund through the Arthur B. McDonald Canadian Astroparticle Physics Research Institute. This work is supported by Subatomic Physics Discovery Grants (individual) from the Natural Sciences and Engineering Research Council of Canada.

References

- [1] C.D. Kreisch, F.-Y. Cyr-Racine and O. Doré, *Neutrino puzzle: Anomalies, interactions, and cosmological tensions*, *Phys. Rev. D* **101** (2020) 123505 [[1902.00534](#)].
- [2] A. Das and S. Ghosh, *Flavor-specific interaction favors strong neutrino self-coupling in the early universe*, *JCAP* **07** (2021) 038 [[2011.12315](#)].
- [3] A. He, R. An, M.M. Ivanov and V. Gluscevic, *Self-interacting neutrinos in light of large-scale structure data*, *Phys. Rev. D* **109** (2024) 103527 [[2309.03956](#)].
- [4] D. Camarena, F.-Y. Cyr-Racine and J. Houghteling, *Confronting self-interacting neutrinos with the full shape of the galaxy power spectrum*, *Phys. Rev. D* **108** (2023) 103535 [[2309.03941](#)].
- [5] A. Das and S. Ghosh, *The magnificent ACT of flavor-specific neutrino self-interaction*, *JCAP* **09** (2023) 042 [[2303.08843](#)].
- [6] D. Camarena and F.-Y. Cyr-Racine, *Absence of concordance in a simple self-interacting neutrino cosmology*, [2403.05496](#).
- [7] S. Pal, R. Samanta and S. Pal, *Exploring neutrino interactions in light of present and upcoming galaxy survey*, [2409.03712](#).
- [8] D. Racco, P. Zhang and H. Zheng, *Neutrino masses from large-scale structures: future sensitivity and theory dependence*, [2412.04959](#).
- [9] A. De Gouvêa, M. Sen, W. Tangarife and Y. Zhang, *Dodelson-Widrow Mechanism in the Presence of Self-Interacting Neutrinos*, *Phys. Rev. Lett.* **124** (2020) 081802 [[1910.04901](#)].

- [10] K.J. Kelly, M. Sen, W. Tangarife and Y. Zhang, *Origin of sterile neutrino dark matter via secret neutrino interactions with vector bosons*, *Phys. Rev. D* **101** (2020) 115031 [[2005.03681](#)].
- [11] K.J. Kelly, M. Sen and Y. Zhang, *Intimate Relationship between Sterile Neutrino Dark Matter and ΔN_{eff}* , *Phys. Rev. Lett.* **127** (2021) 041101 [[2011.02487](#)].
- [12] R. An, V. Gluscevic, E.O. Nadler and Y. Zhang, *Can Neutrino Self-interactions Save Sterile Neutrino Dark Matter?*, *Astrophys. J. Lett.* **954** (2023) L18 [[2301.08299](#)].
- [13] C. Benso, T. Schwetz and D. Vatsyayan, *Large neutrino mass in cosmology and keV sterile neutrino dark matter from a dark sector*, *JCAP* **04** (2025) 054 [[2410.23926](#)].
- [14] P. Parashari, V. Gluscevic, Y. Zhang, S. Bird, M.M. Ivanov and A. He, *Ly α forest bounds on sterile neutrino production via neutrino self-interactions*, [2602.17821](#).
- [15] M. Bauer, P. Foldenauer and J. Jaeckel, *Hunting All the Hidden Photons*, *JHEP* **07** (2018) 094 [[1803.05466](#)].
- [16] T. Ferber, A. Grohsjean and F. Kahlhoefer, *Dark Higgs bosons at colliders*, *Prog. Part. Nucl. Phys.* **136** (2024) 104105 [[2305.16169](#)].
- [17] R. Laha, B. Dasgupta and J.F. Beacom, *Constraints on New Neutrino Interactions via Light Abelian Vector Bosons*, *Phys. Rev. D* **89** (2014) 093025 [[1304.3460](#)].
- [18] J.M. Berryman et al., *Neutrino self-interactions: A white paper*, *Phys. Dark Univ.* **42** (2023) 101267 [[2203.01955](#)].
- [19] J.M. Berryman, A. De Gouvêa, K.J. Kelly and Y. Zhang, *Lepton-Number-Charged Scalars and Neutrino Beamstrahlung*, *Phys. Rev. D* **97** (2018) 075030 [[1802.00009](#)].
- [20] W.F.L. Hollik, *Radiative Corrections in the Standard Model and their Role for Precision Tests of the Electroweak Theory*, *Fortsch. Phys.* **38** (1990) 165.
- [21] H.-C. Cheng and I. Low, *TeV symmetry and the little hierarchy problem*, *JHEP* **09** (2003) 051 [[hep-ph/0308199](#)].
- [22] M.J. Ramsey-Musolf and S. Su, *Low Energy Precision Test of Supersymmetry*, *Phys. Rept.* **456** (2008) 1 [[hep-ph/0612057](#)].
- [23] J. Haller, A. Hoecker, R. Kogler, K. Mönig, T. Peiffer and J. Stelzer, *Update of the global electroweak fit and constraints on two-Higgs-doublet models*, *Eur. Phys. J. C* **78** (2018) 675 [[1803.01853](#)].
- [24] K. Harigaya, E. Petrosky and A. Pierce, *Precision electroweak tensions and a dark photon*, *JHEP* **07** (2024) 201 [[2307.13045](#)].
- [25] E. Bertuzzo, C. Csaki and F. Huller, *Electroweak Precision Constraints on Dark Photon Models with Generalized Mixing*, [2507.16888](#).
- [26] PIENU collaboration, *Search for three body pion decays $\pi^+ \rightarrow l^+ \nu X$* , *Phys. Rev. D* **103** (2021) 052006 [[2101.07381](#)].

- [27] NA62 collaboration, *Search for K^+ decays to a muon and invisible particles*, *Phys. Lett. B* **816** (2021) 136259 [[2101.12304](#)].
- [28] I. Esteban, S. Pandey, V. Brdar and J.F. Beacom, *Probing secret interactions of astrophysical neutrinos in the high-statistics era*, *Phys. Rev. D* **104** (2021) 123014 [[2107.13568](#)].
- [29] S. Foroughi-Abari, K.J. Kelly and Y. Zhang, *Radiative Correction from Secret Neutrino Interactions and Implications for Neutrino-Scattering Experiments*, [2510.15023](#).
- [30] Y. Zhang, *Neutrino self-interaction and weak mixing-angle measurements*, *Phys. Rev. D* **112** (2025) 035027 [[2411.05070](#)].
- [31] H. Flacher, M. Goebel, J. Haller, A. Hocker, K. Monig and J. Stelzer, *Revisiting the Global Electroweak Fit of the Standard Model and Beyond with Gfitter*, *Eur. Phys. J. C* **60** (2009) 543 [[0811.0009](#)].
- [32] GFITTER collaboration, *Updated Status of the Global Electroweak Fit and Constraints on New Physics*, *Eur. Phys. J. C* **72** (2012) 2003 [[1107.0975](#)].
- [33] W.J. Marciano, *Fermi constants and 'New Physics'*, *Phys. Rev. D* **60** (1999) 093006 [[hep-ph/9903451](#)].
- [34] A. Sirlin, *Radiative Corrections in the $SU(2)_L \times U(1)$ Theory: A Simple Renormalization Framework*, *Phys. Rev. D* **22** (1980) 971.
- [35] J. Erler and M.J. Ramsey-Musolf, *Low energy tests of the weak interaction*, *Prog. Part. Nucl. Phys.* **54** (2005) 351 [[hep-ph/0404291](#)].
- [36] ALEPH, DELPHI, L3, OPAL, SLD, LEP ELECTROWEAK WORKING GROUP, SLD ELECTROWEAK GROUP, SLD HEAVY FLAVOUR GROUP collaboration, *Precision electroweak measurements on the Z resonance*, *Phys. Rept.* **427** (2006) 257 [[hep-ex/0509008](#)].
- [37] SLD collaboration, *A High precision measurement of the left-right Z boson cross-section asymmetry*, *Phys. Rev. Lett.* **84** (2000) 5945 [[hep-ex/0004026](#)].
- [38] W.J. Marciano and A. Sirlin, *Radiative Corrections to Neutrino Induced Neutral Current Phenomena in the $SU(2)_L \times U(1)$ Theory*, *Phys. Rev. D* **22** (1980) 2695.
- [39] P. Gambino and A. Sirlin, *Relation between $\sin^2 \theta_w(m(z))$ and $\sin^2 \theta_w^{\text{effective}}(\text{leptonic})$* , *Phys. Rev. D* **49** (1994) 1160 [[hep-ph/9309326](#)].
- [40] CDF, D0 collaboration, *Tevatron Run II combination of the effective leptonic electroweak mixing angle*, *Phys. Rev. D* **97** (2018) 112007 [[1801.06283](#)].
- [41] ATLAS collaboration, *Measurement of the effective leptonic weak mixing angle using electron and muon pairs from Z-boson decay in the ATLAS experiment at $\sqrt{s} = 8$ TeV*, .
- [42] CMS collaboration, *Measurement of the Drell–Yan forward-backward asymmetry and of the effective leptonic weak mixing angle in proton-proton collisions at $s=13$ TeV*, *Phys. Lett. B* **866** (2025) 139526 [[2408.07622](#)].

- [43] LHCb collaboration, *Measurement of the forward-backward asymmetry in $Z/\gamma^* \rightarrow \mu^+\mu^-$ decays and determination of the effective weak mixing angle*, *JHEP* **11** (2015) 190 [[1509.07645](#)].
- [44] S. Foroughi-Abari, K.J. Kelly, M. Rai and Y. Zhang, *Enabling Strong Neutrino Self-Interaction with an Unparticle Mediator*, *Phys. Rev. Lett.* **134** (2025) 181001 [[2501.02049](#)].
- [45] CDF collaboration, *Precise measurement of the W -boson mass with the CDF II detector*, *Phys. Rev. Lett.* **108** (2012) 151803 [[1203.0275](#)].
- [46] D0 collaboration, *Measurement of the W Boson Mass with the D0 Detector*, *Phys. Rev. Lett.* **108** (2012) 151804 [[1203.0293](#)].
- [47] ATLAS collaboration, *Measurement of the W -boson mass and width with the ATLAS detector using proton–proton collisions at $\sqrt{s} = 7$ TeV*, *Eur. Phys. J. C* **84** (2024) 1309 [[2403.15085](#)].
- [48] G.-C. Cho, K. Hagiwara, Y. Matsumoto and D. Nomura, *The MSSM confronts the precision electroweak data and the muon $g-2$* , *JHEP* **11** (2011) 068 [[1104.1769](#)].
- [49] V. Brdar, M. Lindner, S. Vogl and X.-J. Xu, *Revisiting neutrino self-interaction constraints from Z and τ decays*, *Phys. Rev. D* **101** (2020) 115001 [[2003.05339](#)].
- [50] BMW collaboration, *Lattice QCD at the physical point: light quark masses*, *Phys. Lett. B* **701** (2011) 265 [[1011.2403](#)].
- [51] FERMILAB LATTICE, MILC, TUMQCD collaboration, *Up-, down-, strange-, charm-, and bottom-quark masses from four-flavor lattice QCD*, *Phys. Rev. D* **98** (2018) 054517 [[1802.04248](#)].
- [52] M. Awramik, M. Czakon, A. Freitas and G. Weiglein, *Precise Prediction for the W Boson Mass in the Standard Model*, *Phys. Rev. D* **69** (2004) 053006 [[hep-ph/0311148](#)].
- [53] M. Awramik, M. Czakon and A. Freitas, *Electroweak two-loop corrections to the effective weak mixing angle*, *JHEP* **11** (2006) 048 [[hep-ph/0608099](#)].
- [54] A. Freitas, *Higher-order electroweak corrections to the partial widths and branching ratios of the Z boson*, *JHEP* **04** (2014) 070 [[1401.2447](#)].
- [55] PARTICLE DATA GROUP collaboration, *Review of particle physics*, *Phys. Rev. D* **110** (2024) 030001.
- [56] K.M. Nollett and G. Steigman, *BBN And The CMB Constrain Light, Electromagnetically Coupled WIMPs*, *Phys. Rev. D* **89** (2014) 083508 [[1312.5725](#)].
- [57] S.-P. Li and X.-J. Xu, *N_{eff} constraints on light mediators coupled to neutrinos: the dilution-resistant effect*, *JHEP* **10** (2023) 012 [[2307.13967](#)].
- [58] V.D. Barger, W.-Y. Keung and S. Pakvasa, *Majoron Emission by Neutrinos*, *Phys. Rev. D* **25** (1982) 907.

- [59] N. Blinov, K.J. Kelly, G.Z. Krnjaic and S.D. McDermott, *Constraining the Self-Interacting Neutrino Interpretation of the Hubble Tension*, *Phys. Rev. Lett.* **123** (2019) 191102 [[1905.02727](#)].
- [60] P.S.B. Dev, D. Kim, D. Sathyan, K. Sinha and Y. Zhang, *New laboratory constraints on neutrinophilic mediators*, *Phys. Lett. B* **868** (2025) 139765 [[2407.12738](#)].
- [61] C.H. de Lima, D. McKeen, J. Ng and D. Tuckler, *Hadronic Probes of Non-Standard Neutrino Interactions*, [2601.06248](#).
- [62] J. Heintze et al., *A Measurement of the $K^+ \rightarrow e^+$ Neutrino gamma Structure Decay*, *Nucl. Phys. B* **149** (1979) 365.
- [63] PARTICLE DATA GROUP collaboration, *Leptonic Decays of Charged Pseudoscalar Mesons*, .
- [64] P. Coloma, M.C. Gonzalez-Garcia, M. Maltoni, J.P. Pinheiro and S. Urrea, *Global constraints on non-standard neutrino interactions with quarks and electrons*, *JHEP* **08** (2023) 032 [[2305.07698](#)].
- [65] J. Kriewald, M. Nemevšek and F. Nesti, *Enabling precise predictions for left-right symmetry at colliders*, *Eur. Phys. J. C* **84** (2024) 1306 [[2403.07756](#)].
- [66] J. Schechter and J.W.F. Valle, *Neutrino Masses in $SU(2) \times U(1)$ Theories*, *Phys. Rev. D* **22** (1980) 2227.
- [67] G. Lazarides, Q. Shafi and C. Wetterich, *Proton Lifetime and Fermion Masses in an $SO(10)$ Model*, *Nucl. Phys. B* **181** (1981) 287.
- [68] T.P. Cheng and L.-F. Li, *Neutrino Masses, Mixings and Oscillations in $SU(2) \times U(1)$ Models of Electroweak Interactions*, *Phys. Rev. D* **22** (1980) 2860.
- [69] R.N. Mohapatra and G. Senjanovic, *Neutrino Masses and Mixings in Gauge Models with Spontaneous Parity Violation*, *Phys. Rev. D* **23** (1981) 165.
- [70] J. Schechter and J.W.F. Valle, *Neutrino Decay and Spontaneous Violation of Lepton Number*, *Phys. Rev. D* **25** (1982) 774.
- [71] A. Melfo, M. Nemevsek, F. Nesti, G. Senjanovic and Y. Zhang, *Type II Seesaw at LHC: The Roadmap*, *Phys. Rev. D* **85** (2012) 055018 [[1108.4416](#)].
- [72] N.D. Barrie and S.T. Petcov, *Lepton Flavour Violation tests of Type II Seesaw Leptogenesis*, *JHEP* **01** (2023) 001 [[2210.02110](#)].
- [73] ATLAS collaboration, *Search for doubly charged Higgs boson production in multi-lepton final states using 139 fb^{-1} of proton–proton collisions at $\sqrt{s} = 13 \text{ TeV}$ with the ATLAS detector*, *Eur. Phys. J. C* **83** (2023) 605 [[2211.07505](#)].
- [74] L. Guedes, G. Hoff, F.S. Queiroz, Y.M. Oviedo-Torres and Y. Villamizar, *Search for a Doubly Charged Scalar at the LHC and FCC-hh*, [2601.00083](#).
- [75] A. Banerjee, D. Das, S. Mukherjee and S. Pandey, *Drell-Yan constraints on charged scalars: A weak isospin perspective*, *Phys. Rev. D* **111** (2025) 115014 [[2501.09796](#)].

- [76] M.E. Peskin and T. Takeuchi, *A New constraint on a strongly interacting Higgs sector*, *Phys. Rev. Lett.* **65** (1990) 964.
- [77] M.E. Peskin and T. Takeuchi, *Estimation of oblique electroweak corrections*, *Phys. Rev. D* **46** (1992) 381.
- [78] I. Maksymyk, C.P. Burgess and D. London, *Beyond S, T and U*, *Phys. Rev. D* **50** (1994) 529 [[hep-ph/9306267](#)].
- [79] E.J. Chun, H.M. Lee and P. Sharma, *Vacuum Stability, Perturbativity, EWPD and Higgs-to-diphoton rate in Type II Seesaw Models*, *JHEP* **11** (2012) 106 [[1209.1303](#)].
- [80] S. Mandal, O.G. Miranda, G. Sanchez Garcia, J.W.F. Valle and X.-J. Xu, *Toward deconstructing the simplest seesaw mechanism*, *Phys. Rev. D* **105** (2022) 095020 [[2203.06362](#)].
- [81] Y. Cheng, X.-G. He, F. Huang, J. Sun and Z.-P. Xing, *Electroweak precision tests for triplet scalars*, *Nucl. Phys. B* **989** (2023) 116118 [[2208.06760](#)].
- [82] L. Lavoura and L.-F. Li, *Making the small oblique parameters large*, *Phys. Rev. D* **49** (1994) 1409 [[hep-ph/9309262](#)].
- [83] PIONEER collaboration, *European Strategy for Particle Physics Update – PIONEER: a next generation rare pion decay experiment*, [2504.06375](#).